A CMEMS forecasting system for the marine ecosystem of IBI European waters

Elodie Gutknecht[1], Guillaume Reffray[1], Alexandre Mignot[1], Tomasz Dabrowski[2], and Marcos G. Sotillo[1,3]

[1] Mercator Ocean, Parc Technologique du Canal, 8-10 rue Hermes, 31520 Ramonville St-Agne, France
[2] Marine Institute, Rinville, Oranmore, Co. Galway, H91 R673, Ireland
[3] Puertos del Estado, Av. Partenón, 10, 28042 Madrid, Spain

Correspondence to: Elodie Gutknecht (elodie.gutknecht@mercator-ocean.fr)

Abstract. As part of the Copernicus Marine Environment Monitoring Service (CMEMS), an operational ocean forecasting system was developed to monitor the ocean dynamics and marine ecosystems of the European waters; and more specifically on the IBI (Iberia-Biscay-Ireland) area. The CMEMS IBI physical-biogeochemical coupled system covers the North-East Atlantic Ocean from the Canary Islands to Iceland, including the North Sea and the Western Mediterranean, with a NEMO-PISCES 1/36° model application. Since its operational launch in April 2018, this CMEMS IBI system has provided a weekly short-term (7-days) forecast of the ocean dynamics and key biogeochemical variables of the marine ecosystem.

The main goal of this paper is to assess the performances of the IBI biogeochemical system, using a 7-year retrospective simulation that spans from 2010 to 2016. The model results are validated with available satellite and *in situ* observations from the International Council for the Exploration of the Sea (ICES), the European Marine Observation and Data Network (EMODnet) and the Biogeochemical-Argo float network. The simulation successfully reproduces the spatial distribution and seasonal cycles of oxygen, nutrients, chlorophyll-a, and net primary production. This simulation can be a useful tool to better understand the current state and changes in the marine biogeochemistry of European waters. It can also provide key variables for developing indicators to monitor the health of European marine ecosystems. These indicators may be of interest to scientists, policy makers, environmental agencies and the general public.

1 Introduction

The marine ecosystem of the North-East Atlantic waters is subject to natural climate variability as well as intense human pressures that can have significant impacts for the ecosystem. In addition to intense fishing activity, human pressures also include aquaculture, agriculture, maritime transport, oil and gas extraction, tourism, and urbanization. In order to regulate, sustainably manage, protect, and conserve the maritime areas of the North-East Atlantic waters, fifteen governments and the European Union have adopted the OSPAR Convention in 1992. To go further, Europe Union also wants to develop its operational and autonomous Earth observation capacity to serve the general European interest and help public authorities and other international organizations to improve the quality of life. In this objective, the Copernicus European Programme, formerly known as GMES (Global Monitoring for Environment and Security), manages Earth monitoring data from satellite observations, *in situ* measurements and numerical models on water, air and land. Its marine component is the Copernicus

Marine Environment Monitoring Service (CMEMS; http://www.marine.copernicus.eu), implemented and operated by Mercator Ocean International, a service provider of ocean information in real and delayed time (http://www.mercator-ocean.eu). Gathering three kinds of data (satellite, *in situ* and models), CMEMS provides regular and systematic information on the state and variability of the ocean dynamics and marine ecosystems for the global ocean and the European regional

5　seas. The CMEMS service covers the European seas by defining six different areas: Arctic Ocean, Baltic Sea, European North-West Shelf Seas, Black Sea, Mediterranean Sea and Iberia–Biscay–Ireland Seas. Concerning the latter region, the CMEMS Iberia–Biscay–Ireland Monitoring and Forecasting Center (IBI-MFC) is in charge of delivering physical and biogeochemical forecast products over the IBI region. The IBI-MFC Team in charge of the development, production and the later validation of the products works on a model domain using a curvilinear grid, called IBI Extended Domain, covering

10　part of the North-East Atlantic Ocean from the Canary Islands to Iceland, the North Sea and the Western Mediterranean (Fig. 1a). However the IBI-MFC delivers IBI products to CMEMS end-users on a regular grid over a smaller area, called IBI Service Domain, extending from -19°E to 5°E and 26°N to 56°N (Fig. 1a). Further details on the IBI-MFC and the IBI region definition are available in Sotillo et al. (2015).

In addition to have a very high level of human activity, the IBI waters are home to a wide range of physical and

15　biogeochemical oceanic processes that must be understood in order to manage the area accordingly. In this objective, a physical-biogeochemical coupled model system predicts the physical and ecosystem dynamics. The IBI NEMO-PISCES model application, developed by Mercator Ocean, is based on the latest version of the NEMO modelling platform (Madec et al., 1998; Madec, 2008), version 3.6, with a horizontal resolution of 1/36°. The PISCES biogeochemical model simulates the lower trophic levels of the marine food web, from nutrients to mesozooplankton (Aumont et al., 2015). This regional coupled

20　system is hereinafter referred to as IBI36.

The IBI36 operational system provides, since April 2018, on a weekly basis a short-term (7-days) forecast of the ocean dynamics as well as the main biogeochemical variables (oxygen, nutrients, chlorophyll-a, hereinafter denoted Chl-a, and primary production) of the marine ecosystem. A weekly update of physical and biogeochemical hindcast products (generated for the previous week) is also delivered as best historical estimates. The IBI36 system is described and evaluated in the

25　CMEMS documents: Sotillo et al. (2018) for physics and Bowyer et al. (2017) for biogeochemistry.

This paper assesses the performances of the biogeochemical component in reproducing the main biogeochemical variables, using a 7-year retrospective simulation that covers the 2010-2016 period. Despite some of the areas presented here are outside of the IBI Service Domain (where the IBI-MFC delivers IBI products to CMEMS end-users), the model is evaluated over the IBI Extended Domain in order to take advantage of the *in situ* observation coverage.

30　The paper is organized as follows. Section 2 presents an overview of the IBI European seas with emphasis on the main drivers of the ecosystem dynamics. Section 3 describes the IBI36 coupled configuration, the model initialization and boundary conditions, the external forcing, the regional adaptations and the data used for evaluation. In Sect. 4, the biogeochemical tracers are compared to satellite and *in situ* observations. Finally, a discussion and conclusions are provided in Sect. 5.

2 IBI European waters

Phytoplankton dynamics is controlled by the complex interaction between ocean dynamics, nutrients and light availability. In the IBI European waters, phytoplankton dynamics follows a seasonal cycle typical of temperate seas, governed by the alternation between winter mixing and summer stratification of the water column (Barton et al., 2015). A rapid increase in

5   phytoplankton biomass starts in spring, when seasonal re-stratification begins and, when the Mixed Layer Depth (MLD) becomes shallower (Sverdrup 1953; Behrenfeld 2010; Taylor and Ferrari 2011). This event, called spring bloom, is followed by a summer decrease in biomass, when the increase in stratification of the water column reduces the vertical supply of nutrient to the euphotic layer (the layer where phytoplankton grows) (Barton et al., 2015).

In the North-East Atlantic Ocean, primary productivity increases from south to north as a result of the main surface

10   circulation. Near 50°W, the Gulf Stream splits into the North Atlantic Current (NAC) flowing northeastward and the Azores Current (AC) flowing east-southeastward (Rossby, 1996). The meandering Subpolar Front, an extension of the NAC, is a relatively wide region separating the subtropical gyre from the subpolar gyre (Rossby, 1996). In the subtropical North Atlantic, wind stress induces Ekman downwelling that deepens the nutricline, and the warm waters maintain a stratification of the water column throughout the year (Barton et al., 2015). The annual primary production is then limited its seasonal

15   variations are limited. Moving to the subpolar North Atlantic, the seasonal surface cooling deepens the mixed layer in winter, and winds drive Ekman upwelling and make the nutricline shallower (Barton et al., 2015). However, light supply limits the phytoplankton growth in winter. A strong spring bloom is triggered by water column re-stratification in spring, while during summer the stratification limits the nutrient supply to the surface (Williams et al. 2000). This seasonal upward flow of deep and nutrient-rich waters triggers a higher productivity and a strong seasonal cycle.

20   Moving toward the coast, Moroccan and Iberian upwelling systems are part of the Canary Current Upwelling System, one of the four main Eastern Boundary Upwelling Systems of the world, and thus a very productive ecosystem and an active fishery (Aristegui et al., 2004). The season for upwelling along the Iberian coast begins in May-June with the establishment of northerly winds and continues throughout the summer (June-September; Wooster et al., 1976; Nykjær and Van Camp, 1994), with periods of downwelling associated with wind relaxations (Torres and Barton, 2007). Along the Moroccan coasts,

25   upwelling intensifies from the north where it is highly seasonal, with higher activity in the summer and autumn, to the south where it can be considered permanent and intense, with maximum activity from April to September (Pelegrí and Benazzouz, 2015).

The IBI European waters also cover part of the Western Mediterranean Sea. From a biogeochemical perspective, the Mediterranean Sea shows a high N:P ratio (N:P ~ 20 for the western basin; Ribera d'Alcalà et al., 2003), and relatively high

30   oxygen consumption rates compared to the Atlantic and Pacific Oceans (Christensen et al., 1989; Roether and Well, 2001). Mediterranean Outflow Water (MOW) flows into the Gulf of Cadiz and the Atlantic through a sill depth of only 290 meters at the Strait of Gibraltar. This salty and denser water flows out at the bottom of the sill and a northward-moving MOW core

spreads on the continental slope of Portugal at 1000 meters depth, enters the Bay of Biscay, and follow the shelf break further north.

The Bay of Biscay and Celtic Seas are moderately productive ecosystems (UNEP LME report). The seasonal cycle of phytoplankton in the Bay of Biscay is typical of temperate seas (Fernández and Bode, 1991; Valdés et al., 1991; Lavín et al.,

5   2006) but spatial variability is high. The bay is characterized by a weak anticyclonic circulation in the oceanic part, a coastal upwelling, the northerly flow of MOW (OSPAR, 2000; Lavín et al., 2006) and river discharges (Gohin et al., 2003). In the oceanic part of the bay, one biomass peak can be observed in spring due to oligotrophic conditions. However, in the coastal part of the bay, phytoplankton remains relatively high during winter for isobaths less than 100 meters in the Region Of Freshwater Influences (ROFI).

10   The continental shelf widens in the Bay of Biscay. It is quite narrow along the Spanish coast, but increases rapidly with latitude along the French coasts, from 10 km in the south to more than 200 km wide in the north of the bay. The most extensive continental shelf areas are in the Celtic Seas and the North Sea. The continental shelf along the European coasts is the site of intense tidal amplitude and turbulent mixing that prevent stratification (Piraud et al., 2003; Lam et al., 2003, Lavín et al., 2006). To the west of the Celtic Seas, a significant and permanent front can be observed in Chl-a at the edge of the

15   shelf, extending from the northern Bay of Biscay to the Faroe-Shetland Channel, and associated with the shelf edge current (Belkin et al., 2009; Aquarone et al., 2008). The English Channel, connecting the North Sea to the Atlantic, is generally mixed and strongly influenced by winds. The North Sea is characterized by significant river discharges and permanently mixed water column in the south, supplying the highest coastal primary production rates. The north part is characterized by a seasonal stratification and a deep channel in the north-east. Finally, as eastern boundary of the IBI36 domain, the Skagerrak

20   and Kattegat connect the North Sea to the Baltic Sea.

Discharges of fresh and nutrient-rich water from rivers are a strong forcing factor for European waters. In addition to natural inputs related to the watershed erosion, many European coastal ecosystems are damaged by eutrophication due to human activities such as wastewater, agriculture and fish farming (Valdés and Lavin 2002). Eutrophication affects coastal areas, fjords and estuaries, mainly within the Celtic Seas, the Bay of Biscay and the Iberian Coast (OSPAR, 2003). Excessive

25   nutrient enrichment, usually due to increased nitrogen and phosphorous concentrations in rivers, leads to high primary production rates and reduced oxygen concentrations in the bottom water. Oxygen deficiency was reported in the bottom waters of the North-West European shelf (OSPAR, 2013; Ciavatta et al., 2016) and can be used as indicator of the health of marine ecosystems.

3 The IBI36 configuration

30   ### 3.1 The coupled model system

Within the framework of CMEMS, the IBI-MFC Team has deployed an operational forecast service based on a coupled physical-biogeochemical model application. The model domain covers part of the North-East Atlantic Ocean from the

Canary Islands (26°N) to Iceland (64°N), and from 20°W to North Sea (14°E) and the Western Mediterranean (10°E), using a curvilinear grid (Fig. 1a) with a horizontal resolution of 1/36° (~2 km for latitudes covered by the IBI domain) and 50 vertical levels.

The physical model is based on the NEMO 3.6 hydrodynamic model (Madec et al., 1998; Madec, 2008), developed by the
5   NEMO consortium. The NEMO modelling system is freely available (http://www.nemo-ocean.eu), and specific regional improvements include time-splitting and non-linear free surface to correctly simulate high frequency processes such as tides. The ocean dynamics is constrained through data assimilation of *in situ* and satellite physical data (temperature and salinity vertical profiles, sea surface height and sea surface temperature). The IBI36 physical component is described in Sotillo et al. (2018).

10   The biogeochemical model PISCES v2 (Aumont et al., 2015), which is part of the NEMO 3.6 modelling platform, is an intermediary complexity model taking into account 24 prognostic variables. There are five nutrients that limit phytoplankton growth: nitrate and ammonium, phosphate, silicate and iron. Phosphate and nitrate + ammonium are linked by a constant C/N/P Redfield ratio (122/16/1; Takahashi et al., 1985) in all organic compartments of PISCES. The model distinguishes two phytoplankton size compartments (nanophytoplankton and diatoms), for which the prognostic variables are the total biomass
15   in carbon, iron, Chl-a, and silicon (the latter only for diatoms). Consequently, Fe/C, Chl/C, and Si/C ratios are variable and predicted by the model. Two zooplankton size classes (microzooplankton and mesozooplankton) are considered, with constant ratios. The total biomass in C is therefore the only prognostic variable for zooplankton. The bacterial pool is not explicitly modelled. PISCES distinguishes three non-living pools for organic carbon: small particulate organic carbon, big particulate organic carbon and semi-labile dissolved organic carbon. Although the C/N/P composition of dissolved and
20   particulate materials is related to Redfield stoichiometry, the iron content of the particles is computed prognostically. In addition to the three organic detrital pools, particles of calcium carbonate (calcite) and biogenic silicate are modelled. In addition, the model simulates the carbonate system (dissolved inorganic carbon and total alkalinity) and dissolved oxygen. Biogeochemical parameters are based on the standard parameters of PISCES v2. Please refer to Aumont et al. (2015) for the full description of the model.

25   Although PISCES was originally designed for global ocean applications, the distinction of two phytoplankton size classes and the description of multiple nutrient co-limitations allow the model to represent ocean productivity and biogeochemical cycles in the major ocean biogeographic provinces (Longhurst, 1998). PISCES has been successfully used in various biogeochemical studies at global and regional scales, at low and high spatial resolutions as well as for short-term and long-term analyses (e.g. Bopp et al., 2005; Gehlen et al., 2006, 2007; Schneider et al., 2008; Steinacher et al., 2010; Tagliabue et
30   al., 2010, Séférian et al., 2013; Gutknecht et al., 2016). PISCES is also the biogeochemical model used for the IBI reanalysis product (Bowyer et al., 2018), the global ocean analysis and forecast product (Perruche et al., 2016) and the non-assimilative hindcast product (Perruche et al., 2018), all of them are developed at Mercator Ocean for delivery to CMEMS.

For this regional configuration, physics and biogeochemistry are running simultaneously ("on-line" coupling), with the same 1/36° spatial resolution. For reason of numerical cost, the numerical scheme for biogeochemical processes is forward in time

(Euler) while the physical component uses the leap-frog scheme. To respect the conservation of the tracers, the coupling between biogeochemical and physical components is done every other time. The time step of the biogeochemical model is therefore twice that of the physical component, i.e. 900 s. The advection scheme for biogeochemistry is the same QUICKEST scheme (Leonard, 1979) used for the physical part, but using the limiter of Zalezak (1979).

5 **3.2 Model initialization, external forcing and boundary conditions.**

The physical-biogeochemical coupled simulation starts on January 6, 2010 and continues until real time as the model currently provides 7-day weekly ocean forecasts for CMEMS. In this paper, only the first 7 years of simulation (until December 31, 2016) is analysed.

The variables characterizing ocean dynamics (temperature, salinity, currents, and free surface) are initialized and forced to
10 the open boundaries by the daily outputs of the CMEMS global ocean analysis and forecasting system at 1/12° (Lellouche et al., 2016, Lellouche et al., 2018). Both regional and global systems are forced every 3 hours with atmospheric fields from the ECMWF.

The biogeochemistry is initialized with the CMEMS global ocean analysis and forecasting system at ¼° horizontal resolution (Perruche et al., 2016) for the same date. Open boundary conditions come from this same global product on a weekly basis.
15 The global biogeochemical system is also forced by the coarsened global physical outputs mentioned just above, making the different components of CMEMS consistent.

Other boundary fluxes account for the external supply of nutrients (N, P, Si, Fe) and carbon from three different sources: atmospheric dust deposition, rivers and marine sediment mobilization. For more details on external nutrient supplies, please refer to Aumont et al. (2015).
20 Two adaptations are necessary in order to meet regional specificities. The first adaptation concerns vertical sedimentation. In PISCES, external input fluxes are compensated by a loss to sediments in the form of particulate organic matter, biogenic silica and CaCO3. These fluxes correspond to the matter definitely lost to the ocean system. The compensation of external input fluxes by the loss at the lower limit closes the mass balance of the model. While this balance is a valid assumption at the scale of the global ocean, it is not necessarily achieved at the regional level. In addition, strong tidal currents prevent
25 organic matter from settling on the bottom and being stored in the sediments of much of the North-West European continental shelf (De Haas et al., 2002). Thus, no loss to sediment is taken into account in the IBI36 system. The second adaptation concerns the supply of nutrients from rivers. To have a more realistic system, two types of inputs are considered. Natural inputs are injected into the model in the form of surface runoff in the river plumes but also along the coast, using the annual climatology at ½° spatial resolution Global News 2 (Mayorga et al., 2010) which reproduces a realistic hydrology for
30 the year 2000. Additional (anthropic) inputs of nitrates and phosphates are introduced into the system at source points, and are linked to the physical flow. These additional nutrients come from rivers monitored and listed by the European Environment Agency (www.eea.europa.eu) on the basis of annual averages. For the other variables, a reminder of the initial conditions is given.

3.3 Satellite and *in situ* observational data sources used for model validation

This paper evaluates the capacity of the IBI36 system to reproduce the surface and vertical distributions, as well as seasonal cycles of the main biogeochemical variables (Chl-a, primary production, nutrients, oxygen). The model results are thus

5 compared with satellite and *in situ* observational data. Chl-a concentrations and primary productivity are derived from remote sensing estimations. Dissolved oxygen, nutrients (nitrates, phosphates, silicate, and ammonium) and Chl-a concentrations are gathered in regional databases such as ICES (International Council for the Exploration of the Sea), EMODnet (European Marine Observation and Data Network), and the Biogeochemical-Argo floats.

Chl-a concentration is estimated from ocean colour sensors. The regional ESA Ocean Colour CCI product for the North

10 Atlantic and Arctic Oceans with a resolution of 1 km is distributed via CMEMS. The product merges multiple sensors: SeaWiFS, MODIS-Aqua, MERIS and VIIRS. ESA OC-CCI surface Chl-a concentrations (in mg Chl m^{-3}) is estimated from the OC5CI regional algorithm case1/case2, a combination of OCI (Hu et al., 2012) and OC5 (Gohin et al., 2008.). A combined algorithm is required because wide and shallow North-West European shelf seas are supplied in sediment and organic material by many estuaries, which makes the water turbid and disturbs the measurement of Chl-a concentrations.

15 Optically absorbent constituents other than Chl-a are responsible for large uncertainties in coastal ocean colour estimations (up to 100% uncertainty, compared to 30% for open ocean; Moore et al., 2009). A detailed description of the ESA OC-CCI processing system can be found in Sathyendranath et al. (2012).

Concerning net primary production estimates, we use three primary production products distributed by the Oregon State University (www.science.oregonstate.edu/ocean.productivity): the Vertically Generalized Production Model (VGPM;

20 Behrenfeld and Falkowski, 1997; usually recognized as the Standard product), an "Eppley" version of the VGPM product and the Carbon-based Production Model (CbPM; Westberry et al. 2008). These global ocean estimates are monthly averages with a resolution of 1/6°, and are expressed in mg C m^{-2} d^{-1}. Due to the high uncertainty in production products (Henson et al., 2010; Emerson, 2014), PISCES primary production estimates are compared with the three products mentioned above.

The International Council for the Exploration of the Sea (ICES) oceanographic database (www.ices.dk/marine-data/data-

25 portals) gathers quality-controlled *in situ* observational data for the North-East Atlantic Ocean, the North Sea, the Baltic Sea and the Arctic Ocean. Dissolved oxygen, nitrate, phosphate, silicate, ammonium are all expressed in μmol l^{-1}, and Chl-a in mg Chl m^{-3}. Over the period of the IBI36 simulation, ICES data are mainly located in the shallow and coastal waters of the Northern seas.

The European Marine Observation and Data Network (EMODnet) collects, validates, and provides access to relevant marine

30 chemistry data to assess the state of ecosystems in accordance with the Marine Strategy Framework Directive. EMODnet Chemistry has adopted and adapted SeaDataNet standards and services. Regional aggregated products are available for the North-East Atlantic and the Mediterranean (www.emodnet-chemistry.eu/products). The North-East Atlantic Ocean regional product is aggregated, standardized and quality controlled by IFREMER / IDM / SISMER - Scientific Information Systems

7

for the SEA (2018) from France, and the Mediterranean Sea product by Hellenic Centre for Marine Research, Hellenic National Oceanographic Data Centre (HCMR/HNODC) (2018) from Greece. The OVIDE section between Portugal and Greenland in spring 2010 and PELGAS cruises each spring on the Bay of Biscay are part of the North-East Atlantic product. The regional products contain oxygen, nitrate, phosphate, silicate and ammonium profiles all in µmol l^{-1}, and Chl-a profiles

5   in mg Chl m^{-3}. PELGAS Chl-a data come from Niskin bottles.

Biogeochemical-Argo (BGC-Argo) floats are autonomous profiling floats advected by currents (Biogeochemical-Argo Planning Group, 2016). These floats acquire vertical profiles of temperature, salinity, and key biogeochemical variables over complete seasonal cycles. In this study, we use the vertical profiles of dissolved oxygen, nitrate (both estimated in µmol kg^{-1}) and Chl-a concentrations (in mg Chl m^{-3}) collected with 2 BGC-Argo floats in the IBI region. The first float is an APEX

10   profiler (World Meteorological Organization (WMO) number 5904479), deployed in the North Atlantic Ocean by the University of Washington (Seattle) in February 2014 and active until December 2017. The second float is a PROVOR-II profiler (WMO number 6901648), deployed in the Western Mediterranean Sea by the French Villefranche Oceanographic Laboratory in July 2014 and recovered in May 2016. The float data can be downloaded from the Argo Global Data Assembly Centre in France (ftp://ftp.ifremer.fr/ifremer/argo; Carval, et al., 2017). The CTD and trajectory data are quality-

15   controlled following Wong et al. (2015). The raw BGC signals are transformed into Chl-a, oxygen and nitrate concentrations following Schmechtig et al. (2015), Thierry et al. (2016) and Johnson et al. (2016), respectively. Finally, corrections are applied on each variable to correct from calibration biases and sensor drifts. The APEX float observations are adjusted following Johnson et al (2017) and the PROVOR float observations are adjusted following Mignot et al. (2018).

4. IBI36 evaluation

20   The skills of the model are estimated by comparing model results to satellite and *in situ* observations between 2010 and 2016. Chl-a concentration is expressed in in mg Chl m^{-3}, net primary production is expressed in mg C m^{-2} d^{-1}, and oxygen and nutrient concentrations, for standardization purposes, are converted in µmol l^{-1}. The spatial distributions of ICES, EMODnet and BGC-Argo data are presented in Fig. 1b. In function of data availability, the spatial distribution, seasonal cycle and statistics performance are presented.

25   ### 4.1 Satellite estimations

Satellite data are scarce north of 50°N during the winter season, especially between November and February due to omnipresent cloud coverage that dramatically limits the observation of Chl-a concentrations. Consequently, the model is masked based on data availability. The annual average is calculated using the 7 years of simulation. Time series, Hovmöller diagrams and time correlation are based on monthly averages. The time series are presented for several small boxes. The first

30   four are located offshore and the others follow the coastal areas from North to South.

4.1.1 Chlorophyll-a

Predicted sea surface Chl-a concentration is compared to ESA OC-CCI estimates (Fig. 2). On annual average, the large-scale distribution of Chl-a is correctly reproduced: the North Atlantic subtropical gyre with low surface concentrations (< 0.1 mg Chl m^{-3}), increasing concentrations when moving to the north, and the highest values on the continental shelf. The Chl-a

5   signature of the shelf-slope front is well marked west of the British Isles to the Faroe-Shetland Channel. The maximum coastal Chl-a is supplied by nutrient input from rivers, resuspension by strong tidal currents in the Northern shelf, and upwelling off the Iberian and Moroccan coasts. Major biases are located on the continental shelf (Fig. 2c). The model simulates a higher annual average in the northern part (southern North Sea, English Channel, Irish Sea), the Bay of Biscay, the Alboran Sea, and the ROFI of the Ebro and Rhone rivers. The model underestimates Chl-a concentrations off the coast of

10   Morocco (south of Agadir) and in the region linking the North Sea to the Baltic Sea (Kattegat and Skagerrak) (Fig. 2c).

The simulated seasonal cycle is in phase with satellite estimates, particularly south of 50°N, in view of the strong temporal correlation (Fig. 2d). The Hovmöller diagram at 15°W catches the North Atlantic spring phytoplankton bloom, expressed as Chl-a (Fig. 3). A Chl-a peak develops in March in the southern part of the domain and gradually moves northward. The bloom onset is well reproduced in the south, but it spreads more rapidly to the north. The observed peak reaches Iceland in

15   summer (June-July) while the simulated peak reaches Iceland in May. The summer decrease after the bloom is then earlier and sometimes more pronounced in the model, explaining the alternation of positive and negative biases in the Hovmöller diagram at 15°W (Fig. 3c) and the lower temporal correlation to the north of the domain (Fig. 2d). But one part of the seasonal dynamics is also missing due to cloud cover masking several months each winter.

Figure 4 presents the time series of surface Chl-a concentrations in 12 small boxes. In general, the model predicts the

20   seasonal cycle of Chl-a quite well. South of 50°N, coastal ecosystems of the Bay of Biscay (box 7), the upwelling off Portugal and Morocco (boxes 8 and 9), the Gulf of Cadiz, the Alboran Sea and the Gulf of Lions (boxes 10, 11 and 12) succeed in reproducing the seasonal cycle of Chl-a (Fig. 4), with a high correlation coefficient between the model and the data. In shallow Northern seas, the model do not match satellite estimates (Fig. 4; see boxes 4, 5 and 6, respectively, the open North Sea, southern North Sea and English Channel); the spring bloom is in phase but not the rest of the year. High

25   simulated surface concentrations persist in summer in the English Channel and the southern North Sea, while remote sensing data predict a sharp decrease after the spring bloom.

4.1.2 Net primary production

Ocean depth integrated Net Primary Productivity (NPP) is compared to the three primary production products (VGPM, Eppley-VGPM and CbPM; Fig. 5). On annual average, the IBI36 system (Fig. 5d) provides for a NPP of 230 gC m^{-2} yr^{-1} at

30   the western boundary of the domain that gradually increases towards the coasts. The highest NPP (1700 gC m^{-2} yr^{-1}) is found in the coastal regions of the North Sea, where rivers and mixed water columns supply the euphotic layer with nutrients. Compared to the Standard VGPM product (Fig. 5a), the IBI36 system underestimates the NPP by a factor of 2 on average

over the domain. This underestimation reaches a factor of 3-4 on the European coasts. The most important differences concern the Kattegat and the Skagerrak. The spatial distribution of simulated NPP is in between the Eppley-VGPM and CbPM products instead (Fig. 5c).

Figure 6 presents the time series of NPP in the same 12 small boxes as for Chl-a. The seasonal cycle of NPP is generally in line with the VGPM-based products. The very good correlation in the south part of the Atlantic (r=0.91 with the VGPM) decreases northward, as IBI36 predicts a moderate and earlier production peak. In addition, the second peak, or at least the maintenance of high NPP in summer, is not reproduced. The seasonal cycle is very similar in the shallow Northern seas (boxes 4 to 6) and in all coastal waters of the simulated domain (Fig. 6). The correlation is low compared to the CbPM product, the latter giving a seasonal cycle distinct from the VGPM-based products.

Spatial distribution and time series highlight the high variability of NPP products (Fig. 5 and 6). The VGPM is the most productive product. A well-defined cross-shore gradient and the highest seasonal amplitude characterize it. The Eppley-VGPM behaves the same way as the VGPM, but less productive. The CbPM is the less productive, with the lowest coastal production, a more uniform rate over a large part of the domain including the open ocean, and a less pronounced seasonal cycle, sometimes out of phase with VGPM-based products (boxes 3, 11 and 12; the subtropical gyre, Gibraltar strait and Gulf of Cadiz; Fig. 6).

Campbell et al. (2002) pointed out that the "best-performing algorithms generally fall within a factor of 2 of the estimates derived from ^{14}C", and NPP products have poor performances for water columns with depths less than 250 meters (Saba et al., 2011). Schourup-Kristensen et al. (2012) also reported that the VGPM product is twice as productive as biogeochemical models along the European coasts. This high uncertainty in NPP products prevents a quantitative assessment. We can therefore only say that the simulated NPP lies between the three NPP products. IBI36 is in between the Eppley-VGPM and CbPM in terms of spatial distribution, and better correlated to the VGPM-based products with regard to seasonal variations.

4.2 *In situ* historical data

For comparison to ICES and EMODnet databases, the daily averages of the modelled data are co-located with *in situ* data at the point closest of the model grid at the surface and using linear interpolation on the vertical dimension. ICES data are mainly located in the shallow and coastal waters of the Northern seas where nutrients inputs from rivers are significant (Fig. 1b). EMODnet regional products cover the Western Mediterranean Sea, the open Atlantic with OVIDE section between Portugal and Greenland during spring 2010, and the Bay of Biscay with PELGAS cruises in each year during May (Fig. 1b).

4.2.1 Northern Seas

Shallow Northern seas are assessed using oxygen, nutrients and Chl-a from ICES database. Dispersion diagrams for the full set of match-ups are presented on Fig. 7. Sea surface spatial distribution and seasonal cycle are on Fig. 8 and 9.

The oxygen match-ups are well aligned along the bisector with a very good correlation of 0.81 indicating that the model reproduces the amplitude and variability of the observations (Fig. 7). The temporal evolution at the sea surface (Fig. 9)

confirms the realistic amplitude and phase. Oxygen is slightly overestimated in the North Sea and English Channel, with an average bias of 10.7 µmol l^{-1} (corresponding to a percent bias of 4%) (Fig. 8). In addition, the model does not capture the lower oxygen pool than that measured during 2014-2015 period (see the pool of overestimated oxygen in Fig. 7 and 9). This anomaly is located in the region linking the North Sea to the Baltic Sea (Kattegat and Skagerrak), the eastern boundary of the

5   domain.

Ciavatta et al. (2016) worked on continental shelf areas vulnerable to oxygen deficiency, defining deficiency when at least one daily value is below the 6 mg l^{-1} (187.5 µmol l^{-1}) threshold. Using the same definition, ICES data and the IBI36 system identify vulnerable areas in the North Sea and in particular its eastern part (Fig. 10). The seasonal cycle of the minimum oxygen levels are well correlated (r=0.77). The waters are oxygenated in winter while they can deplete below the 2 µmol l^{-1}

10   threshold or even reach anoxic conditions in summer (Fig. 10). But ICES data only permit identifying the North Sea because the data density strongly decreases outside. So extending this analysis to the full set of simulated oxygen, minimum levels are also predicted in the Celtic Seas, Armorican shelf, coastal areas of Scotland and Western Ireland. Ciavatta et al. (2016) and the OSPAR commission point out these aforementioned regions as eutrophication problem areas, and Breitburg et al (2018) also report low and declining oxygen levels in almost all coastal waters of the North-West European shelf.

15   Following this positive oxygen assessment, the IBI36 system can therefore be used to monitor the surface area exposed to oxygen deficiency. Using the same method as Ciavatta et al. (2016), the IBI36 system predicts a maximum extension of 280 000 km^2 by considering at least one daily value below the threshold. Vulnerable areas are similar to those reported by Ciavatta et al. (2016), while Celtic Seas and the English Channel are less affected. The seasonal extension varies from a very restricted and oxygenated surface are in winter to an average surface area of 85 000 km^2 in summer (Fig. 10), associated with

20   deoxygenated waters that can reach anoxic conditions in the North Sea and along the west coats of France.

The distribution of nitrates is also well represented with a high correlation of 0.84 (Fig. 7). The model generally underestimates surface nitrate with an average bias of -1 µmol l^{-1} (9.6% percent bias) (Fig. 8). The time series shows a seasonal cycle in phase, but excessive nitrate concentrations are simulated in spring and summer when the observed concentrations are very low (Fig. 9). Very high values of 100 to 300 µmol l^{-1} are simulated throughout the year in the

25   vicinity of river flows between the Rhine and Elbe. They are not visible on the dispersion diagram (Fig. 7) because a filter eliminates low-density points. But on other hand, these extreme values have an impact on the smoothed time series (Fig. 9). The negative bias observed in space is masked in the time series by extreme values.

Phosphate and silicate are overestimated for low concentrations during spring-summer seasons, while higher concentrations during winter conditions are better captured (Fig. 7 and 9). The phosphate dispersion diagram shows two high-density zones.

30   The spring-summer overprediction is mainly along the coasts. Winter conditions are better captured, although still a little high. The data show a marked seasonal cycle while simulated phosphate levels remain too high throughout the year. The average bias of 0.22 µmol l^{-1} or 48.3 % percent bias is reduced to 31.5% if the pathway to Baltic Sea is excluded. Silicate has an average bias of 2.1 µmol l^{-1} or 46.8% percent bias. They are overestimated in the open North Sea and underestimated

along the coasts between the Rhine and the Elbe. In addition, percent bias decreases to 30.8% if the pathway to Baltic Sea is excluded.

For ammonium and Chl-a, match-ups show a high dispersion; the model does not reproduce the high variability observed in data (Fig. 7). The seasonal cycle is in phase for Chl-a but out of phase for ammonium (Fig. 9). On the other hand, the

5 magnitude is captured for ammonium but not for Chl-a. Mean Chl-a concentrations along the coasts are underestimated (Fig. 8). The model predicts a slow spring increase instead of a strong bloom in mid-march (Fig. 9). It should be noted that coastal Chl-a appears to be underestimated compared to ICES *in situ* data, whereas it is overestimated compared to satellite estimates (see Sect. 4.1.1 and Fig. 2), which recalls the high uncertainties of remote sensing signal in coastal waters due to interference from Chl-a content and other optically absorbing elements such as suspended matter, coloured dissolved organic

10 matter and bottom reflectance (Moore et al., 2009).

Comparison with the ICES database in the Northern part of the IBI domain shows that the seasonal cycle of nutrients is not sufficiently marked, particularly for phosphate and silicate, and that the high spring bloom is not intense enough. Nutrient and Chl-a patterns are strongly influenced by river nutrient input. In the coupled IBI36 system, nutrient inputs at river points are prescribed using a constant value, while inputs usually follow a seasonal cycle related to precipitation and watershed

15 erosion. In addition, sedimentary processes (i.e. remineralization of organic carbon and subsequent release of nutrients) are not considered here, this assumption may be too restrictive. The Kattegat and Skagerrak are also complicated to reproduce. But the exit from the Baltic Sea is a very specific marine area probably not apprehended by the global product used at boundary.

4.2.2 North-East Atlantic waters

20 North-East Atlantic is evaluated using the OVIDE radial section sampled in June 2010 between Portugal and Greenland (Fig. 11). Oxygen and nutrients correlate very well with OVIDE data, with coefficient correlation higher than 0.95. The model catches the main vertical distribution of biogeochemical tracers. The dispersion diagram for oxygen shows two pools of high density: one for low oxygen values, and the other one for high concentrations. Throughout the OVIDE vertical section, the minimum oxygen level is around 1000 meter deep. Low oxygen content in the eastern part of the section is due to MOW on

25 the shelf of the Iberian Basin. Oxygen maximum around 2500 meters relies on recently ventilated Labrador Sea Water (Garcia-Ibanez et al., 2015) that reaches the western part of the section. The three nutrients present a maximum around 1000 meters, the lower values at this depth being due to MOW. High silicate (45-50 µmol l^{-1}) near the bottom reflects the influence of Antarctic Bottom Water in the North-East Atlantic Ocean (Garcia-Ibanez et al., 2015).

However, vertical profiles are somewhat smoothed. The minimum and maximum oxygen at respectively, 1000 and 2500

30 meters, are not pronounced enough. Also nutrient maximum around 1000 meters is weaker.

Ocean Science

Discussions

Open Access

EGU

4.2.3 Bay of Biscay

The Bay of Biscay is assessed using the PELGAS data (Doray et al., 2018a, 2018b). These data allow evaluating the spring conditions of the bay. Sea surface oxygen concentrations are well correlated with PELGAS data (correlation of 0.74), which means that amplitude and variability are correctly simulated. Simulated concentrations present an average bias of +16.4

5 μmol l^{-1} (corresponding to a percent bias of 6.3%; Fig. 12). Spring nutrient concentrations are realistically simulated, except at the ROFI of French rivers. Surface oxygen bias and excessive nutrient discharges were already highlighted in the North Sea using the ICES database. The surface Chl-a is very close to the data: the cross-shore gradient is realistic with spring concentrations of 0.3 mg Chl m^{-3} offshore, which increase to 6 mg Chl m^{-3} along the French coast.

4.2.4 Mediterranean Sea

10 The Mediterranean Sea is assessed using EMODnet database that has a very good spatial coverage for oxygen and Chl-a tracers, while nutrient data are limited to the northern part of the domain. Oxygen comparison gives the same conclusions as for the North Sea and the Bay of Biscay: the model succeeds in reproducing the amplitude and variability of oxygen, but a constant bias persists. So only the sea surface Chl-a distribution is presented here (Fig. 13). High coastal values are located along the Catalan coast, in the ROFI of the Ebro, along the Costa Blanca and along Algeria. Two highly productive areas are

15 located further offshore: one in the convection zone of the Gulf of Lions and the other in the Algerian Basin between Sardinia and Algeria. Everywhere else, Chl-a is lower. The model simulates Chl-a higher than EMODnet in the Alboran Sea and in the ROFI of the Rhône River. This overestimation was already highlighted by comparison with satellite estimates (see Sect. 4.1.1). EMODnet therefore confirms this tendency. But in a general way, the model reproduces very well the distribution of surface Chl-a in the Mediterranean.

20 ### 4.3 BGC-Argo data

The free-drifting BGC-Argo profiling floats allow continuous monitoring of dissolved oxygen, nitrate and Chl-a of the upper 1000 meters of the ocean. 2 BGC-Argo floats are used here, one in the North Atlantic Ocean and the other in the Western Mediterranean Sea.

Figure 14 shows the density plots between the BGC-Argo floats and simulated fields of oxygen, nitrate and Chl-a

25 concentrations in the two basins. Overall, the model predictions are in good agreement with the BGC-Argo observations with correlation coefficients greater than 0.75 for all variables in the two basins. For all variables, the model shows a gain lower than 0.7, suggesting that the model tends to overestimate low concentrations and underestimate high concentrations of oxygen, nitrate and Chl-a. This is clearly evidenced in Fig. 15 that shows the time evolutions of the vertical sections of oxygen, nitrate and Chl-a estimated from the BGC-Argo floats and the model. In particular, the deep oxygen minimum and

30 nitrate maximum are not pronounced enough in the model. Oxygen remains 20 μmol l^{-1} too high and nitrate 5 μmol l^{-1} too low. The smoothing of the vertical profiles of oxygen and nutrients was already highlighted in the OVIDE section.

Additionally, the model simulates relatively high Chl-a concentrations at depths where there is no light and no phytoplankton is expected, indicating that the parameterization of Chl-a degradation in PISCES could be improved.

The skill of the model in representing the seasonal cycles of oxygen, nitrate and Chl-a concentrations in the Atlantic Ocean and Mediterranean Sea is also evaluated in Fig. 15. In the Atlantic Ocean (Fig. 15, left side), the seasonal cycle of oxygen, nitrate and Chl-a concentrations are dominated by the spring bloom that dramatically increases oxygen and Chl-a concentrations and decrease nitrate concentrations in the surface layer when mixing stops and the MLD becomes shallower in spring, as clearly shown in the float observations. Overall, the model reproduces roughly the timing of the bloom. The intensity of the bloom is misrepresented in the model as Chl-a concentrations remain significantly too low in spring and become rapidly depleted in summer. Additionally, a Deep Chlorophyll Maximum (DCM) not present in the observations develops in the model simulation.

In the Mediterranean Sea (Fig. 15, right side), the seasonal cycles of Chl-a and oxygen are characterized by the formation of a DCM (Mignot et al., 2014; Lavigne et al., 2015) associated to a Deep Oxygen Maximum (DOM) (Estrada et al., 1985) in the lower part of the euphotic layer. These maxima are also associated with the limit between nutrient-depleted and the nutrient-rich layers, termed nitracline (Estrada et al., 1993). The model correctly reproduces the time evolution of the nitracline, depth and intensity of the DCM and DOM from spring to fall.

5 Discussion and conclusions

An extended validation of the model application used as base of the CMEMS IBI-MFC biogeochemical forecast service is provided. The IBI-MFC operational forecast system is based on the NEMO-PISCES modelling platform in its latest version 3.6, with a 1/36° horizontal resolution. It provides weekly a short-term (7-days) forecast of the ocean dynamics as well as the main biogeochemical variables. A weekly update of hindcast products (generated for the week before) is also delivered as part of the product, and configures the historic best estimates. The skills of the IBI36 configuration to reproduce the main biogeochemical variable distribution are assessed using a 7-year retrospective simulation starting in January 2010 up to December 2016.

The model results are evaluated using satellite estimates for Chl-a and net primary production. The annual average and seasonal cycle is described here. *In situ* observations come from ICES, EMODnet and the BGC-Argo float network for oxygen, nutrients and Chl-a concentrations. Observational data are available for the North-East Atlantic waters, the Bay of Biscay, the Northern Seas and the Western Mediterranean. Some of these areas are outside of the IBI Service Domain (that is the geographical domain covered by the CMEMS IBI-MFC products). But in order to take advantage of their *in situ* observational coverage, not only the IBI Service Domain is evaluated here but the IBI Extended Domain instead. *In situ* data allow a detailed assessment to be made in order to understand the strengths and weaknesses of the model, providing the trails for improvement to be explored. They are discussed below.

The large-scale distribution of sea surface Chl-a is correctly reproduced, with no surprising higher biases on the continental shelf. The seasonal cycle in line with satellite estimates, particularly south of 50°N, while the North Atlantic spring phytoplankton bloom spreads more rapidly to the north. Primary production is a complex field to evaluate, as NPP products give widely different estimates among themselves. Simulated NPP lies between the three NPP products. The averaged spatial

5   distribution is in between the Eppley-VGPM and CbPM products, and seasonal variations are better correlated to the VGPM-based products.

Dissolved oxygen obtains very good statistics. The model is able to reproduce the amplitude and variability of the observations in the open Atlantic, the Mediterranean but also on the continental shelf. However, sea surface oxygen is slightly overestimated (around 4%). Surface ocean concentrations tend to balance with atmospheric concentrations, and here

10   atmospheric oxygen concentrations are prescribed by a constant value over time and space. A spatial and temporal atmospheric oxygen forcing would be beneficial instead. As well, the EMODnet and BGC-Argo comparison highlight a smoothing of the vertical oxygen profiles in the wider ocean that can originate from the physical or biogeochemical models. Different approaches are currently under study. Vertical diffusion could explain the loss of peaks and minima in vertical profiles. Biogeochemical processes are also investigated. But the regional model inherits the qualities and weaknesses of the

15   forcing global model, and the latter simulates a smoothed vertical distribution, so this default cannot be caught up in the regional model without improvements in the initial and open boundary conditions.

The distribution of nutrients is also satisfying. In the wider ocean, vertical distribution presents the same default as oxygen one, i.e. the smoothed vertical profiles, already discussed above. In the coastal Northern seas, the seasonal cycle of nutrients is not sufficiently marked. As well, phytoplankton spring bloom is not intense enough. But continental shelf ecosystem of

20   Northern seas is strongly driven by river discharges. Annually averaged nutrient inputs are injected into the ocean system, while a time evolution or at least a seasonal variation would be necessary to apprehend the phytoplankton dynamics. As well, sedimentary processes are neglected in the IBI36 system as strong tidal currents prevent organic matter from reaching and accumulating in sediments. As an alternative a sediment module should be coupled to the biogeochemical model to improve the representation of sedimentary processes, i.e. remineralization of organic carbon and subsequent release of

25   nutrients.

Phytoplankton, oxygen and nitrate dynamics are evaluated using the BGC-Argo floats. In the Mediterranean, a seasonal DCM develops below the MLD, and is associated with a MOC just above the DCM. This is well caught by the model. But the model also simulates a seasonal DCM in the Atlantic around 50°N while maximum Chl-a remains at the surface in BGC-Argo estimates. This DCM lets us suspect a distinct physical or biogeochemical behaviour at 50°N in the Atlantic between

30   the model and the data. The formation of a DCM indicates that phytoplankton production has to deepen in order to reach the nitracline, and it is usually a typical feature of stratified water columns. Here, the physical model assimilates temperature and salinity profiles from Argo float network, so we can not suspect the model to overestimate the influence of stratified water masses of the subtropical gyre at 50°N. Instead, the biogeochemical distribution may constrain phytoplankton to grow deeper to find enough nutrients. However, the validation of the Atlantic part is limited to only one BGC-Argo float measuring

oxygen, nitrate and Chl-a. Additional floats measuring key the biogeochemical variables would be required to understand the seasonal dynamics of phytoplankton, oxygen and nitrate on the Atlantic side.

Finally, the European IBI shelf ecosystem can be exposed to oxygen deficiency. Vulnerable areas are well located in the Northern seas and Bay of Biscay, and seasonal variations are in phase with observations. Maximum surface area can reach

5   280 000 km^2 when considering at least one daily value below the oxygen threshold during the time of the simulation. However, the vulnerable surface area is almost non-existent in winter as waters are well oxygenated due to strong mixing and extends to an average surface area of 85 000 km^2 in summer, associated with deoxygenated waters that can reach anoxic conditions in the North Sea and along the west coats of France. This IBI-MFC biogeochemical forecast service is likely to give rise to an Ocean Monitoring Indicator (OMI). As an IBI-MFC on-going work, it is currently being investigated the

10 design of some IBI biogeochemical OMI, with the aim of publishing it in the context of the CMEMS Ocean State Report publication (von Schuckmann et al., 2016, 2018).

Code availability

The IBI36 configuration is based on the NEMO 3.6 version developed by the NEMO consortium. NEMO modelling system is freely available at http://www.nemo-ocean.eu. The biogeochemical model PISCES v2 is part of the NEMO modelling

15 platform and is available via the NEMO web site. Model initialization and boundary conditions are available via CMEMS (http://www.marine.copernicus.eu).

Data availability

The regional ESA Ocean Colour CCI product for the North Atlantic and Arctic Oceans with a resolution of 1 km is distributed via CMEMS (http://www.marine.copernicus.eu). Primary production products are distributed by the Oregon State

20 University (www.science.oregonstate.edu/ocean.productivity). The International Council for the Exploration of the Sea (ICES) oceanographic database is available at www.ices.dk/marine-data/data-portals. The European Marine Observation and Data Network (EMODnet) is available at www.emodnet-chemistry.eu/products. EMODnet aggregated data products are generated by EMODnet Chemistry under the support of DG MARE Call for Tenders MARE/2008/03-lot3, MARE/2012/10-lot4 and EASME/EMFF/2016/006-lot4. Biogeochemical-Argo (BGC-Argo) float data can be downloaded from the Argo

25 Global Data Assembly Centre in France (ftp://ftp.ifremer.fr/ifremer/argo).

Ocean Science
Discussions

5   **References**

Aquarone, M. C., Adams, S., and Valdes, L.: XIII-37 Celtic-Biscay Shelf: LME #24. In Sherman, K. & Hempel, G. (eds) The UNEP Large Marine Ecosystem Report: A Perspective on Changing Conditions in LMEs of the World's Regional Seas. UNEP Regional Seas Report and Studies No. 182: 527–534. Nairobi: United Nations Environmental Program, 2008.

Aristegui, J., Alvarez-Salgado, X. A., Barton, E. D., Figueiras, F. G., Hernandez-Leon, S., Roy, C., and Santos., A. M. P.:

10 Oceanography and fisheries of the Canary Current/Iberian Region of theeastern North Atlantic, Chapter 23 in The Sea, The Global Coastal Ocean: InterdisciplinaryRegional Studies and Syntheses, 14, A. R. Robinson and K. H. Brink, eds., Harvard UniversityPress, Cambridge, MA, 2004.

Aumont, O., Ethé, C., Tagliabue, A., Bopp , L., and Gehlen, M.: PISCES-v2: an ocean biogeochemical model for carbon and ecosystem studies. Geosci. Model Dev., 8, 2465–2513, http://www.geosci-model-dev.net/8/2465/2015/gmd-8-2465-

15 2015.pdf, 2015.

Barton, A. D., Lozier, M. S. and Williams, R. G.: Physical controls of variability in North Atlantic phytoplankton communities. Limnol. Oceanogr., 60: 181-197. doi:10.1002/lno.10011, 2015.

Behrenfeld, M.: Abandonding Sverdrup's crtical depth hypothesis on phytoplankton blooms. Ecology 91: 977–989. doi:10.1890/09-1207.1, 2010.

20 Behrenfeld, M. J., and Falkowski, P. G.: Photosynthetic rates derived from satellite-based chlorophyll concentration, Limnol. Oceanogr., 42(1), 1-20, 1997.

Belkin, I. M., Cornillon, P. C., and Sherman, K.: Fronts in Large Marine Ecosystems. Progress in Oceanography 81 (1-4), 223–236. doi:10.1016/j.pocean.2009.04.015, 2009.

Biogeochemical-Argo Planning Group: The scientific rationale, design and implementation plan for a Biogeochemical-Argo

25 float array, https://doi.org/10.13155/46601, 2016.

Bopp, L., Aumont, O., Cadule, P., Alvain, S., and Gehlen, M.: Response of diatoms distribution to global warming andpotential implications: A global model study. Geophys. Res. Lett.. 32, L19606, doi:10.1029/2005GL023653, 2005.

Bowyer, P., Dabrowski, T., Gutknecht, E., Lorente, P., Reffray, G., and Sotillo, M. G.: Quality Information Document (CMEMS-IBI-QUID-005-004), http://marine.copernicus.eu/documents/QUID/CMEMS-IBI-QUID-005-004.pdf, 2017.

30 Bowyer, P., Dabrowski, T., Gutknecht, E., Lorente, P., Reffray, G., Sotillo, M.G.: Quality Information Document (CMEMS-IBI-QUID-005-003), http://marine.copernicus.eu/documents/QUID/CMEMS-IBI-QUID-005-003.pdf, 2018.

Breitburg, D., Levin, L. A., Oschlies, A., Grégoire, M., Chavez, F. P., Conley, D. J., Garçon, V., Gilbert, D., Gutiérrez, D., Isensee, K., Jacinto, G. S., Limburg, K. E., Montes, I., Naqvi, S. W. A., Pitcher, G. C., Rabalais, N. N., Roman, M. R., Rose, K. A., Seibel, B. A., Telszewski, M., Yasuhara, M., and Zhang, J.: Declining oxygen in the global ocean and coastal waters, Science, 359 (6371), eaam7240, doi: 10.1126/science.aam7240, 2018.

5 Campbell, J. W., Antoine, D., Armstrong, R., Arrigo, K., Balch, W., Barber, R., Behrenfeld, M., Bidigare, R., Bishop, J., Carr, M.-E., Esaias, W., Falkowski, P., Hoepffner, N., Iverson, R., Kiefer, D., Lohrenz, S., Marra, J., Morel, A., Ryan, J., Vedernikov, V., Waters, K., Yentsch, C., and Yoder, J.: Comparison of algorithms for estimating ocean primary production from surface chlorophyll, temperature, and irradiance, Global Biogeochem. Cycles, 16(3), doi: 10.1029/2001GB001444, 2002.

10 Carval, T., Keeley, R., Takatsuki, Y., Yoshida, T., Schmid, C., Goldsmith, R., Wong, A., McCreadie, R., Thresher, A., Tran, A.: Argo user's manual V3.2. https://doi.org/10.13155/29825, 2017.

Christensen, J. P., Packard, T. T., Dortch, F. Q., Minas, H. J., Gascard, J. C., Richez, C., and Garfield, P. C.: Carbon oxidation in the deep Mediterranean Sea: Evidence for dissolved organic carbon source, Global Biogeochem. Cycles, 3(4), 315–335, doi:10.1029/GB003i004p00315, 1989.

15 Ciavatta, S., Kay, S. Saux-Picart, S. Butenschön, M. and Allen J. I.: Decadal reanalysis of biogeochemical indicators and fluxes in the North West European shelf-sea ecosystem, J. Geophys. Res. Oceans, 121, 1824–1845, doi:10.1002/2015JC011496, 2016.

De Haas, H., Van Weering, T. C. E., and De Stigter, H.: Organic carbon in shelf seas: sinks or sources, processes and products, Continental Shelf Research, 22, 691–717, 2002.

20 Doray, M., Huret, M., Authier, M., Duhamel, E., Romagnan, J.-B., Dupuy, C., Spitz, J., Sanchez, F., Berger, L., Dorémus, G., Bourriau, P., Grellier, P., Pennors, L., Masse, J., Petitgas, P.: Gridded maps of pelagic ecosystem parameters collected in the Bay of Biscay during the PELGAS integrated survey. SEANOE. https://doi.org/10.17882/53389, 2018a.

Doray, M., Petitgas, P., Romagnan, J.-B., Huret, M., Duhamel, E., Dupuy, C., Spitz, J., Authier, M., Sanchez, F., Berger, L., Doremus, G., Bourriau, P., Grellier, P., Masse, J. : The PELGAS survey: ship-based integrated monitoring of the Bay of
25 Biscay pelagic ecosystem. Progress In Oceanography, 166, 15-29, doi: 10.1016/j.pocean.2017.09.015, 2018b.

Emerson, S.: Annual net community production and the biological carbon flux in the ocean, Global Biogeochem. Cy., 28, 14–28, doi:10.1002/2013GB004680, 2014.

Estrada M.: Deep Phytoplankton and Chlorophyll Maxima in the Western Mediterranean. In: Moraitou-Apostolopoulou M., Kiortsis V. (eds) Mediterranean Marine Ecosystems. NATO Conference Series (I Ecology), vol 8. Springer, Boston, MA,
30 1985.

Estrada, M., Marrasé, C., Latasa, M., Berdalet, E., Delgado, M., and Riera, T. : Variability of deep chlorophyll maximum characteristics in the Northwestern Mediterranean. Marine Ecology-progress Series - MAR ECOL-PROGR SER. 92. 289-300. 10.3354/meps092289, 1993.

Fernández, E., and Bode, A.: Seasonal patterns of primary production in the Central Cantabrian Sea (Bay of Biscay). Sci. Mar., 55 (4), 629–636, 1991.

Garcia-Ibanez, M. I., Pardo, P. C., Carracedo, L., Mercier, H., Lherminier, P., Rios, A. F., and Perez F. F.: Structure, transports and transformations of the water masses in the Atlantic Subpolar Gyre. Progress In Oceanography, 135, 18-36., doi: 10.1016/j.pocean.2015.03.009, 2015.

Gehlen, M., Bopp, L., Emprin, N., Aumont, O., Heinze, C., and Ragueneau, O.: Reconciling surface ocean productivity,export fluxes and sediment composition in a global biogeochemical ocean model. Biogeosciences. 1726-4189/bg/2006-3-521,521-537, 2006.

Gehlen, M., Gangstø, R., Schneider, B., Bopp, L., Aumont, O., and Ethé, C.: The fate of pelagic CaCO3 production in a highCO2 ocean: A model study. Biogeosciences., 4: 505-519, 2007.

Gohin, F., Lampert, L., Guillaud, J.-F., Herbland, A., and Nézan, E.: Satellite and in situ observations of a late winter phytoplankton bloom, in the northern Bay of Biscay. Continental Shelf Research. 23. 1117-1141. 10.1016/S0278-4343(03)00088-8, 2003.

Gohin, F., Saulquin, B., Oger-Jeanneret, H., Lozac'h, L., Lampert, L., Lefebvre, A., Riou, P., and Bruchon, F.: Towards a better assessment of the ecological status of coastal waters using satellite-derived chlorophyll-a concentrations, Remote Sensing of Environment, 112, 3329-3340, 10.1016/j.rse.2008.02.014, 2008.

Gutknecht, E., Reffray, G., Gehlen, M., Triyulianti, I., Berlianty, D., and Gaspar, P.: Evaluation of an operational ocean model configuration at 1/12° spatial resolution for the Indonesian seas (NEMO2.3/INDO12) – Part 2: Biogeochemistry, Geosci. Model Dev., 9, 1523-1543, doi:10.5194/gmdd-9-1523-2016, 2016.

Hellenic Centre for Marine Research, Hellenic National Oceanographic Data Centre (HCMR/HNODC): Mediterranean Sea - Eutrophication and Ocean Acidification aggregated datasets 1911/2017 v2018. Aggregated datasets were generated in the framework of EMODnet Chemistry III, under the support of DG MARE Call for Tender EASME/EMFF/2016/006 - lot4, https://doi.org/10.6092/89576629-66d0-4b76-8382-5ee6c7820c7f, 2018.

Henson, S. A., Sarmiento, J. L., Dunne, J. P., Bopp, L., Lima, I., Doney, S. C., John, J., and Beaulieu, C.: Detection of anthropogenic climate change in satellite records of ocean chlorophyll and productivity, Biogeosciences, 7, 621–640, doi:10.5194/bg-7-621-2010, 2010.

Hu, C., Lee, Z., and Franz, B.A.: Chlorophyll-a algorithms for oligotrophic oceans: A novel approach based on three-band reflectance difference, J. Geophys. Res., 117, C01011, doi:10.1029/2011JC007395, 2012.

IFREMER / IDM / SISMER - Scientific Information Systems for the SEA: North East Atlantic Ocean - Eutrophication and Ocean Acidification aggregated datasets 1921/2017 v2018. Aggregated datasets were generated in the framework of EMODnet Chemistry III, under the support of DG MARE Call for Tender EASME/EMFF/2016/006 - lot4, https://doi.org/10.6092/459D8254-6C7B-4A0E-9FDB-04EFFE5F5A77, 2018.

Johnson, K., Pasqueron De Fommervault, O., Serra, R., D'Ortenzio, F., Schmechtig, C., Claustre, H., and Poteau, A.: *Processing Bio-Argo nitrate concentration at the DAC Level* (p.). https://doi.org/10.13155/46121, 2016.

19

Johnson, K. S., Plant, J. N., Coletti, L. J., Jannasch, H. W., Sakamoto, C. M., Riser, S. C., Swift, D. D., Williams, N. L., Boss, E., Haëntjens, N., Talley, L. D., and Sarmiento J. L.: Biogeochemical sensor performance in the SOCCOM profiling float array: SOCCOM BIOGEOCHEMICAL SENSOR PERFORMANCE. *Journal of Geophysical Research: Oceans*, *122*(8), 6416–6436. https://doi.org/10.1002/2017JC012838, 2017.

5   Lam, F. P. A., Gerkema, T., and Maas, L. R. M.: Preliminary results from observations of internal tides and solitary waves in the Bay of Biscay. http://www.whoi.edu/science/AOPE/people/tduda/isww/text/lam/, 2003.

Lavigne, H., D'Ortenzio, F., Ribera D'Alcalà, M., Claustre, H., Sauzède, R., and Gacic, M.: On the vertical distribution of the chlorophyll a concentration in the Mediterranean Sea: a basin-scale and seasonal approach, Biogeosciences, 12, 5021–5039, https://doi.org/10.5194/bg- 12-5021-2015, 2015.

10   Lavín, A., Valdés, L., Sánchez, F., Abaunza, P., Forest, A., Boucher, J., Lazure, P., and Jegou, A.-M. : The Bay of Biscay: the encountering of the ocean and the shelf. In: The Sea. Volume 14. Part B. The Global Coastal Ocean: Interdisciplinary Regional Studies and Synthesis, Edition: First, Chapter: 24, Publisher: Harvard University Press, Editors: A. Robinson, K. Brink, pp.933-999, 2006.

Lellouche, J.-M., Le Galloudec, O., Regnier, C., Levier, B., Greiner, E., and Drevillon, M. : Quality Information Document
15   (CMEMS-GLO-QUID-001-024), http://marine.copernicus.eu/documents/QUID/CMEMS-GLO-QUID-001-024.pdf, 2016.

Lellouche, J.-M., Greiner, E., Le Galloudec, O., Garric, G., Regnier, C., Drevillon, M., Benkiran, M., Testut, C.-E., Bourdalle-Badie, R., Gasparin, F., Hernandez, O., Levier, B., Drillet, Y., Remy, E., and Le Traon, P.-Y.: Recent updates to the Copernicus Marine Service global ocean monitoring and forecasting real-time 1⁄12° high-resolution system, Ocean Sci., 14, 1093-1126, https://doi.org/10.5194/os-14-1093-2018, 2018.

20   Leonard, B. P.: A stable and accurate convective modelling procedure based on quadratic upstream interpolation, Comput. Method. Appl. M., 19, 59–98, 1979.

Longhurst, A.: Ecological geography in the sea. Academic Press, 1998.

Madec, G.: "NEMO ocean engine", Note du Pole de modélisation, Institut Pierre-Simon Laplace (IPSL), France, No 27 ISSN No 1288-1619, 2008.

25   Madec, G., Delecluse, P., Imbard, M., and Lévy, C.: "OPA 8.1 Ocean General Circulation Model reference manual", Note du Pole de modélisation, Institut Pierre-Simon Laplace (IPSL), France, No11, 91pp., 1998.

Mayorga, E., Seitzinger, S. P., Harrison, J. A., Dumont, E., Beusen, A. H. W., Bowman, A. F., Fekete, B. M., Kroeze, C., and Van Drecht, G.: Global Nutrient Export from WaterSheds 2 (NEWS 2): model development and implementation, J. Environ. Modell. Softw., 25, 837–853, 2010.

30   Mignot, A., Claustre, H., Uitz, J., Poteau, A., D'Ortenzio, F., and Xing, X.: Understanding the seasonal dynamics of phytoplankton biomass and the deep chlorophyll maximum in oligotrophic environments: A Bio-Argo float investigation, Global Biogeochemical Cycles, 28, 856–876, https://doi.org/10.1002/2013GB004781, 2014.

Mignot, A., D'Ortenzio, F., Taillandier, V., Cossarini, G., and Salon S.: Quantifying observational errors in Biogeochemical-argo oxygen, nitrate and chlorophyll a concentrations, Submitted to, Geophys. Res. Lett., 2018.

Ocean Science
Discussions

Open Access

EGU

Moore, T. S., Campbell, J. W., and Dowell, M. D: A class-based approach to characterizing and mapping the uncertainty of the MODIS ocean chlorophyll product, Remote Sensing of Environment, 113, 2424-2430, 2009.

Nykjær, L., Van Camp, L.: Seasonal and interannual variability of coastal upwelling along northwest Africa and Portugal from 1981 to 1991. Journal of Geophysical Research, 99(C7):14197, 1994.

5   OSPAR: Quality Status Report 2000: Region IV - Bay of Biscay and Iberian Coast. OSPAR Commission. London. 134 + xiii pp, 2000.

OSPAR: OSPAR integrated report 2003 on the eutrophication status of the OSPAR maritime area based upon the first application of the Comprehensive Procedure. OSPAR Eutrophication Series, publication 189/2003. OSPAR Commission, London, 2003.

10   OSPAR: Common procedure for the identification of the eutrophication status of the OSPAR maritime area, Tech. Rep. 2013-8., London, U. K. [Available at www.ospar.org/documents?d532957], 2013.

Pelegrí, J. L., and Benazzouz, A.: Coastal upwelling off North-West Africa. In: Oceanographic and biological features in the Canary Current Large Marine Ecosystem. Valdés, L. and Déniz-González, I. (eds). IOC-UNESCO, Paris. IOC Technical Series, No. 115, pp. 93-103. URI: http://hdl.handle.net/1834/9180, 2015.

15   Perruche, C., Hameau, A., Paul, J., Régnier, C., and Drévillon M.: Quality Information Document (CMEMS-GLO-QUID-001-014), http://marine.copernicus.eu/documents/QUID/CMEMS-GLO-QUID-001-014.pdf, 2016.

Perruche, C., Szczypta, C., Paul, J., and Drévillon, M.: Quality Information Document (CMEMS-GLO-QUID-001-029), http://marine.copernicus.eu/documents/QUID/CMEMS-GLO-QUID-001-029.pdf, 2018.

Piraud, I., Marseleix, P., and Auclair, F.: Tidal and thermohaline circulation in the Bay of Biscay. Geophys. Res. Abstracts,
20   5, 07058, 2003.

Ribera d'Alcalà, M., Civitarese, G., Conversano, F., and Lavezza, R.: Nutrient ratios and fluxes hint at overlooked processes in the Mediterranean Sea, J. Geophys. Res., 108 (C9), 8106, doi:10.1029/2002JC001650, 2003.

Roether, W., and Well, R.: Oxygen consumption in the Eastern Mediterranean, Deep Sea Res., Part I, 48(6), 1535–1551, 2001.

25   Rossby, T.: The North Atlantic Current and surrounding waters: At the crossroads. Rev. Geophys., 34, 463–481, doi:https://doi.org/10.1029/96RG02214, 1996.

Saba, V. S., Friedrichs, M. A. M., Antoine, D., Armstrong, R. A., Asanuma, I., Behrenfeld, M. J., Ciotti, A. M., Dowell, M., Hoepffner, N., Hyde, K. J. W., Ishizaka, J., Kameda, T., Marra, J., Mélin, F., Morel, A., O'Reilly, J., Scardi, M., Smith Jr., W. O., Smyth, T. J., Tang, S., Uitz, J., Waters, K., and Westberry, T. K.: An evaluation of ocean color model estimates of
30   marine primary productivity in coastal and pelagic regions across the globe, Biogeosciences, 8, 489-503, https://doi.org/10.5194/bg-8-489-2011, 2011.

Sathyendranath, S., Brewin, R. J. W., Müeller, D., Brockmann, C., Deschamps, P.-Y., Doerffer, R., Fomferra, N., Franz, B. A., Grant, M. G., Hu C., Krasemann, H., Lee, Z., Maritorena, S., Devred, E., Mélin, F., Peters, M., Smyth, T., Steinmetz, F.,

Swinton, J., Werdell, J., and Regner, P.: Ocean Colour Climate Change Initiative: Approach and Initial Results, IGARSS 2012, 2024-2027. http://dx.doi.org/10.1109/IGARSS.2012.6350979, 2012.

Schmechtig, C., Poteau, A., Claustre, H., D'Ortenzio, F., and Boss, E.: Processing bio-Argo chlorophyll-A concentration at the DAC level. Ifremer. https://doi.org/10.13155/39468, 2015.

Schneider, B., Bopp, L., Gehlen, M., Segschneider, J., Frölicher, T. L., Cadule, P., Friedlingstein, P., Doney, S. C., Behrenfeld, M. J., and Joos, F.: Climate-induced interannual variability of marine primary and export production in three global coupled climatecarbon cycle models. Biogeosciences. 5: 597-614, 2008.

Schourup-Kristensen, V., Sidorenko, D., Wolf-Gladrow, D. A., and Völker, C.: A skill assessment of the biogeochemical model REcoM2 coupled to the Finite Element Sea-Ice Ocean Model (FESOM 1.3). Geosci. Model Dev. 7: 2769–2802., 2012.

Séférian, R., Bopp, L., Gehlen, M., Orr, J. C., Ethé, C., Cadule, P., Aumont, O., Mélia, D. S. Y., Voldoire, A., and Madec, G.: Skill assessment of three earth system models with common marine biogeochemistry, Clim. Dynam., 40, 2549–2573, doi:10.1007/s00382-012-1362-8, 2013.

Sotillo, M. G., Cailleau, S., Lorente, P., Levier, B., Aznar, R., Reffray, G., Amo-Baladrón, A., Chanut, J., Benkiran, M., and Alvarez-Fanjul, E.: The MyOcean IBI Ocean Forecast and Reanalysis Systems: operational products and roadmap to the future Copernicus Service, Journal of Operational Oceanography, DOI: 10.1080/1755876X.2015.1014663, 2015.

Sotillo, M. G., Levier, B., and Lorente, P.: Quality Information Document (CMEMS-IBI-QUID-005-001), http://marine.copernicus.eu/documents/QUID/CMEMS-IBI-QUID-005-001.pdf, 2018.

Steinacher, M., Joos, F., Frölicher, T. L., Bopp, L., Cadule, P., Cocco, V., Doney, S. C., Gehlen, M., Lindsay, K., Moore, J. K., Schneider, B., and Segschneider, J.: Projected 21st century decrease in marine productivity: a multi-model analysis.Biogeoscience. 7: 979-1005, 2010.

Sverdrup, H.: On conditions of the vernal blooming of phytoplankton. ICES J. Mar. Sci. 18: 287–295. doi:10.1093/icesjms/18.3.287, 1953.

Tagliabue, A., Bopp, L., Dutay, J.-C., Bowie, A. R., Chever, F., Jean-Baptiste, P., Bucciarelli, E., Lannuzel, D., Remenyi, T., Sarthou, G., Aumont, O., Gehlen, M. and Jeandel, C.: On the importance of hydrothermalism to the oceanic dissolved ironinventory. Nature Geoscience. 3: 252 – 256, doi:10.1038/ngeo818, 2010.

Takahashi, T., Broecker, W. S., and Langer, S.: Redfield ratio based on chemical data from isopycnal surfaces, J. Geophys. Res., 90, 6907–6924, 1985.

Taylor, J. R., and Ferrari. R.: Shutdown of turbulent convection as a new criterion for the onset of spring phytoplankton blooms. Limnol. Oceanogr. 56: 2293–2307. doi:10.4319/lo.2011.56.6.2293, 2011.

Thierry, V., Bittig, H., Gilbert, D., Kobayashi, T., Kanako, S., and Schmid, C.: *Processing Argo oxygen data at the DAC level cookbook* (p.). https://doi.org/10.13155/39795, 2016.

Torres, R., and Barton, E. D.: Onset of the Iberian upwelling along the Galician coast. Continental Shelf Research, 27(13):1759–1778, 2007.

Valdés, L., Alvarez-Ossorio, M. T., Lavín, A., Varela, M., and Carballo, R.: Ciclo anual de parámetros hidrográficos, nutrientes y plancton en la plataforma continental de La Coruña (NO, España). Bol. Inst. Esp. Oceanog., 7 (1), 91–138, 1991.

Valdés, L., and Lavin, A.: Dynamics and human impact in the Bay of Biscay: An ecological perspective p 293-320 in:

5   Sherman, K. and Skjoldal, H.R. (eds), Large Marine Ecosystems of the North Atlantic – Changing States and Sustainability. Elsevier Science, Amsterdam, The Netherlands, 2002.

von Schuckmann, K., Le Traon, P.-Y., et al: The Copernicus Marine Environment Monitoring Service Ocean State Report, Journal of Operational Oceanography, 9:sup2, s235-s320, DOI: 10.1080/1755876X.2016.1273446, 2016.

von Schuckmann, K., Le Traon, P.-Y., et al.: Copernicus Marine Service Ocean State Report, Journal of Operational

10   Oceanography, 11:sup1, S1-S142, DOI: 10.1080/1755876X.2018.1489208, 2018.

Westberry, T., Behrenfeld, M. J., Siegel, D. A., and Boss, E.: Carbon-based primary productivity modeling with vertically resolved photoacclimation, Global Biogeochem. Cycles, 22(2), GB2024, doi:10.1029/2007GB003078, 2008.

Williams, R. G., McClaren, A. J., and Follows., M. J.: Estimating the convective supply of nitrate and implied variability in export production over the North Atlantic. Global Biogeochem. Cycles 14: 1299–1313. doi:10.1029/2000GB001260, 2000.

15   Wong, A., Keeley, R., Carval, T., & Argo Data Management Team: Argo Quality Control Manual for CTD and Trajectory Data. https://doi.org/10.13155/33951, 2015.

Wooster, W. S., Bakun, A., Mclain, D. R.: Seasonal Upwelling Cycle Along the Eastern Boundary of the North-Atlantic. Journal of Marine Research, 34(2):131–141, 1976.

Zalezak, S. T.: Fully multidimensional flux-corrected transport algorithms for fluids, J. Computat. Phys., 31, 335–362, 1979.

20
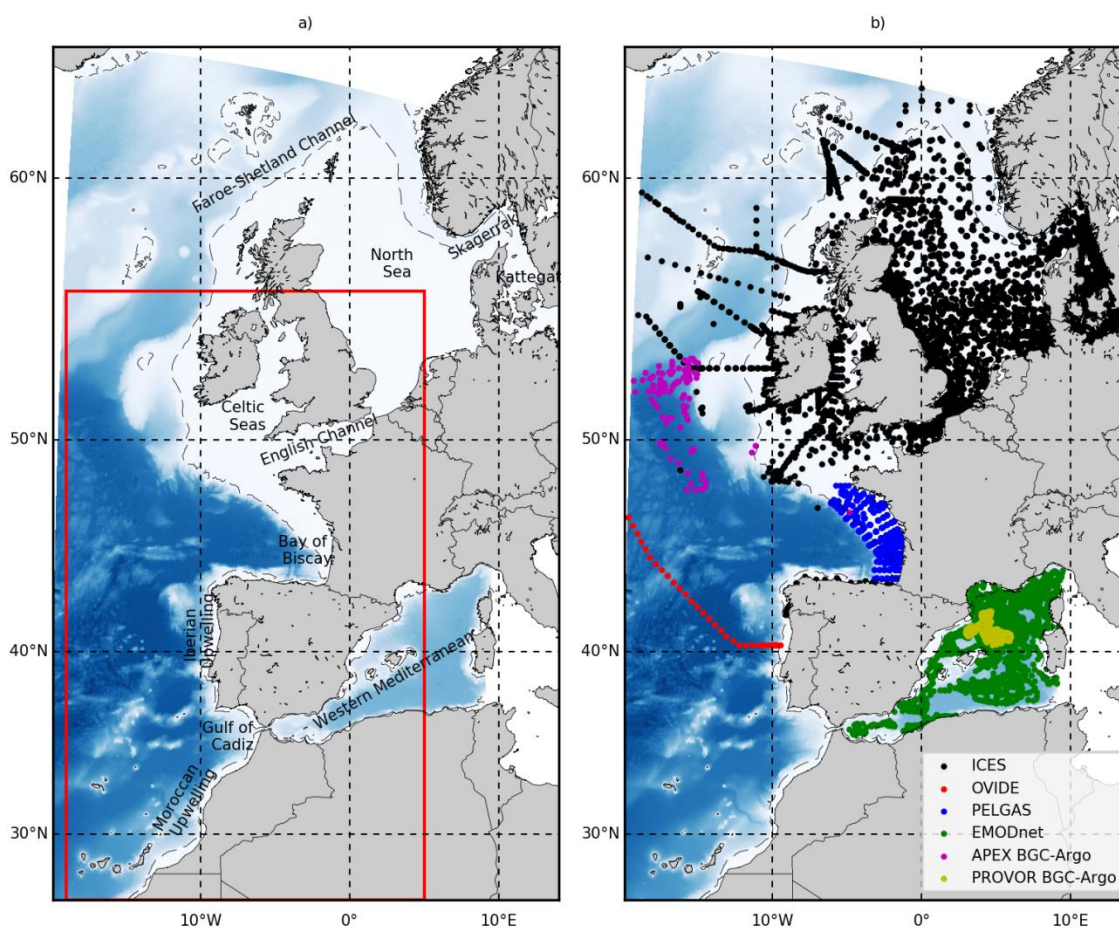
Figure 1. a) IBI Extended Domain on a curvilinear grid and IBI Service Domain extends from -19°E to 5°E and 26°N to 56°N on a regular grid (red rectangle). b) Location of in-situ biogeochemical data used for validation. ICES data are in black, OVIDE section is in red, PELGAS data are in blue, the Mediterranean Sea product of the EMODnet is in green, the APEX BGC-Argo float in the Atlantic is in Magenta, and PROVOR BGC-Argo float in the Mediterranean is in yellow.
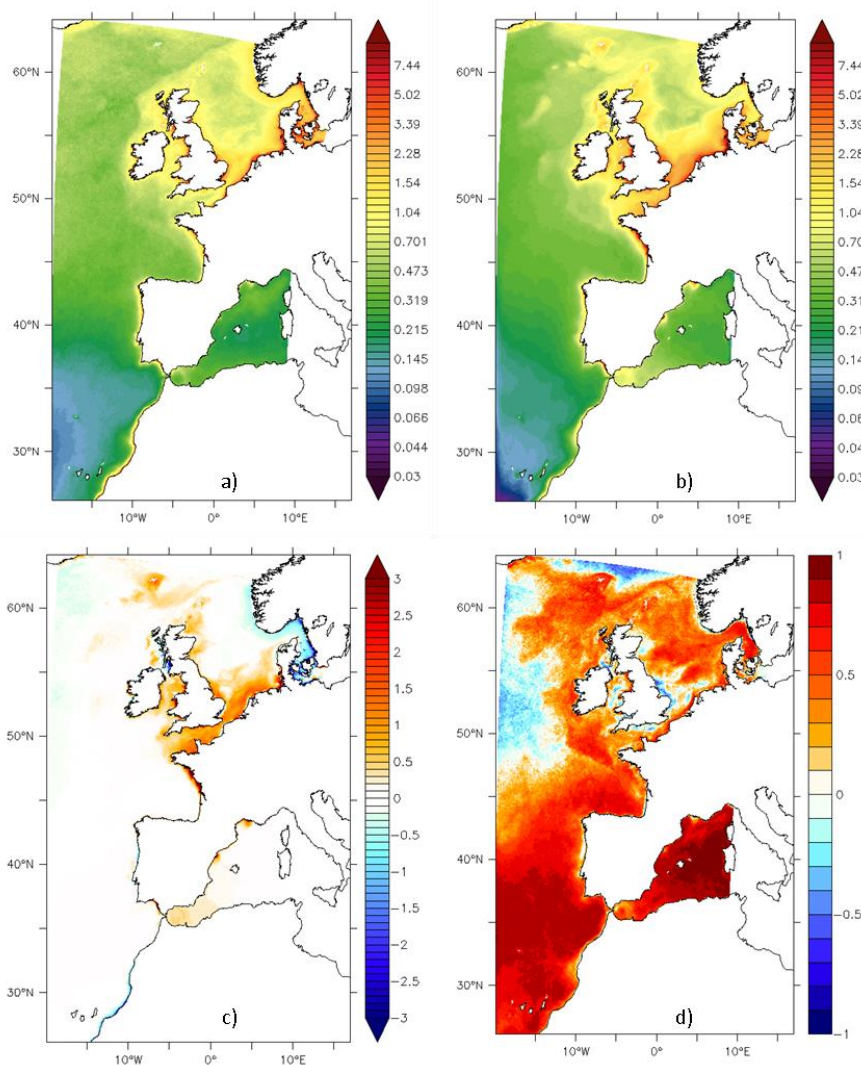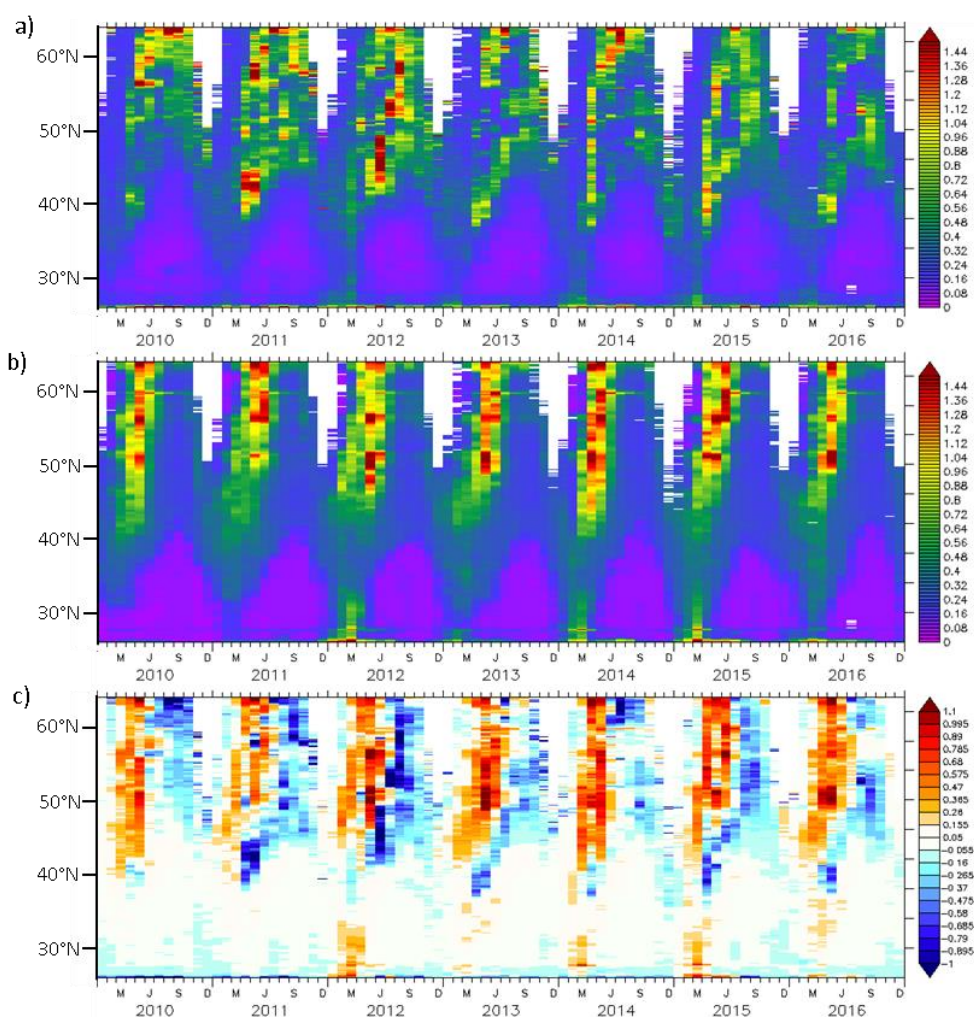
Figure 2. Sea surface Chl-a. a) annual average of ESA OC-CCI ocean colour product, b) annual average of IBI36 and c) averaged bias of Chl-a (model - observation), all expressed in mg Chl m^{-3}. d) Temporal correlation between the model and the observation. Statistics are computed from monthly fields between 2010 and 2016, and the model is masked as a function of the data.

5

Figure 3. Hovmöller diagram for sea surface Chl-a at 15°W between 2010 and 2016. a) ESA OC-CCI ocean colour product, b) IBI36 and c) bias of Chl-a (model - observation), all expressed in mg Chl m^{-3}. The model is masked as a function of the data.
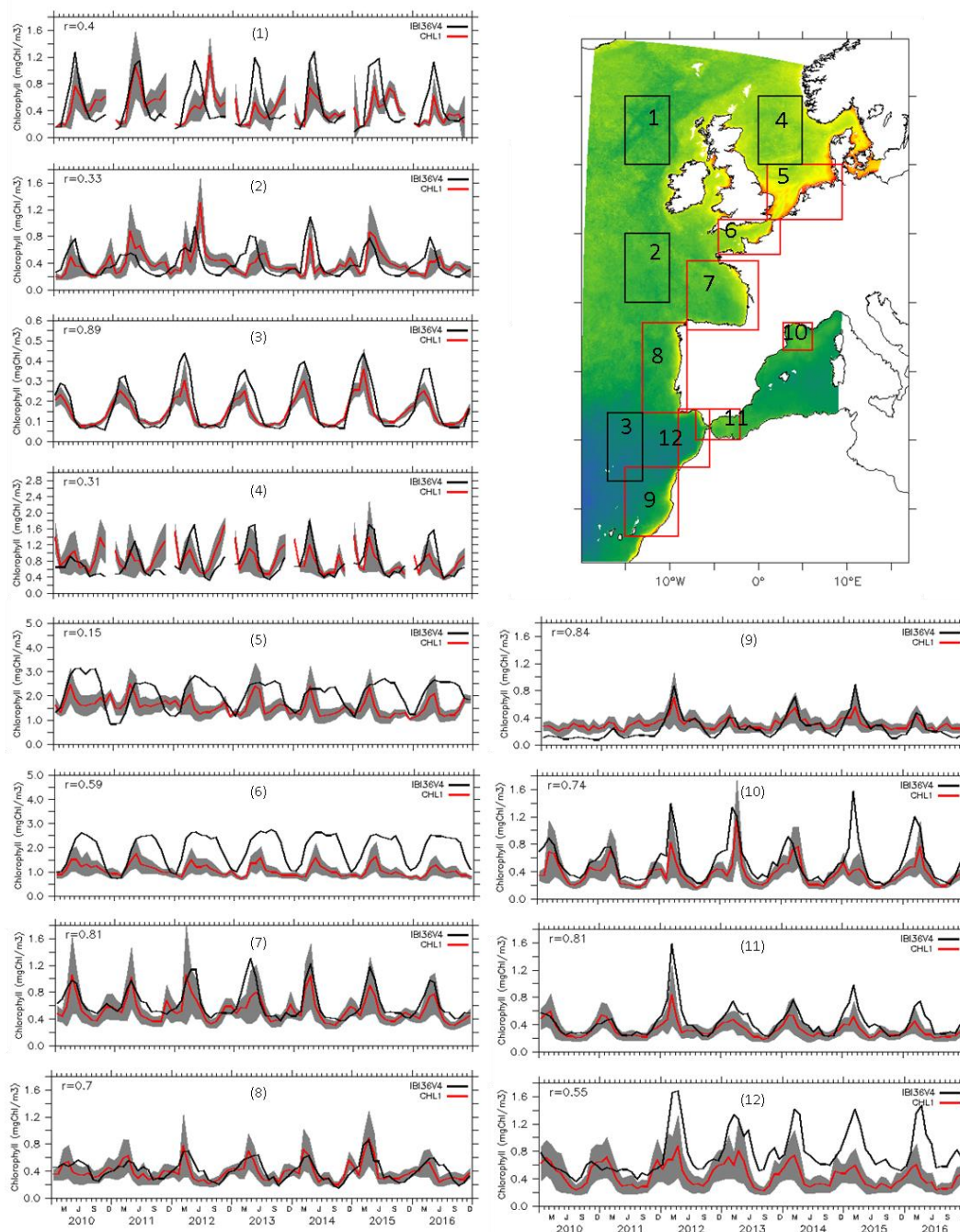
Figure 4. Time series of Sea surface Chl-a (mg Chl m^{-3}) between 2010 and 2016. IBI36 is in black and ESA OC-CCI ocean colour product in red with associated error in grey. Concentrations are averaged over 12 small boxes as defined in the map on the top-right. The model is masked as a function of the data. Note the different scales in y-axis. The correlation between the model and the data is indicated in the top-left of each panel.
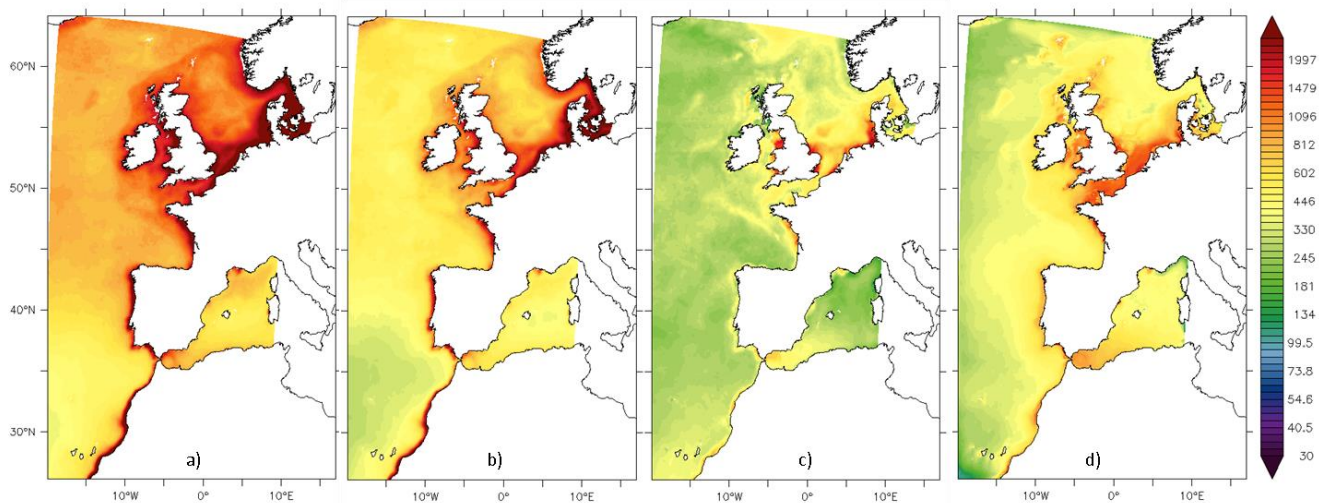
Figure 5. Depth integrated net primary production (mg C m^{-2} d^{-1}). Annual average for a) VGPM, b) Eppey-VGPM, c) CbPM and d) IBI36. Averages are computed from monthly fields between 2010 and 2015, and the model is masked as a function of the data.
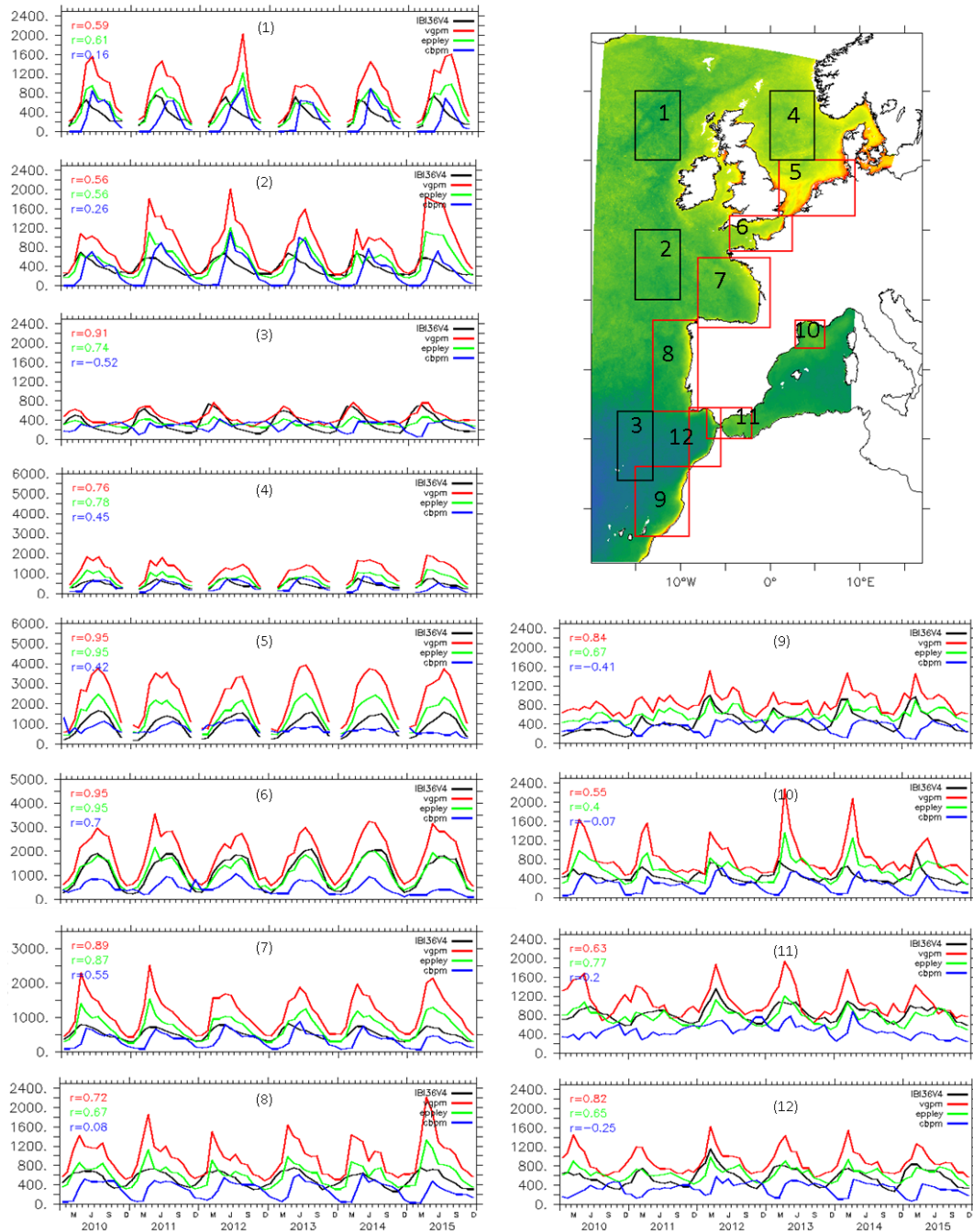
Figure 6. Time series of depth integrated net primary production (mg C m^{-2} d^{-1}) between 2010 and 2015. IBI36 is in black, VGPM in red, Eppey-VGPM in green and CbPM in blue. NPP is averaged over 12 small boxes as defined in the map on the top-right. The model is masked as a function of the data. Note the different scales in y-axis. The correlation between the model and the NPP products (using corresponding colours) is indicated in the top-left of each panel.
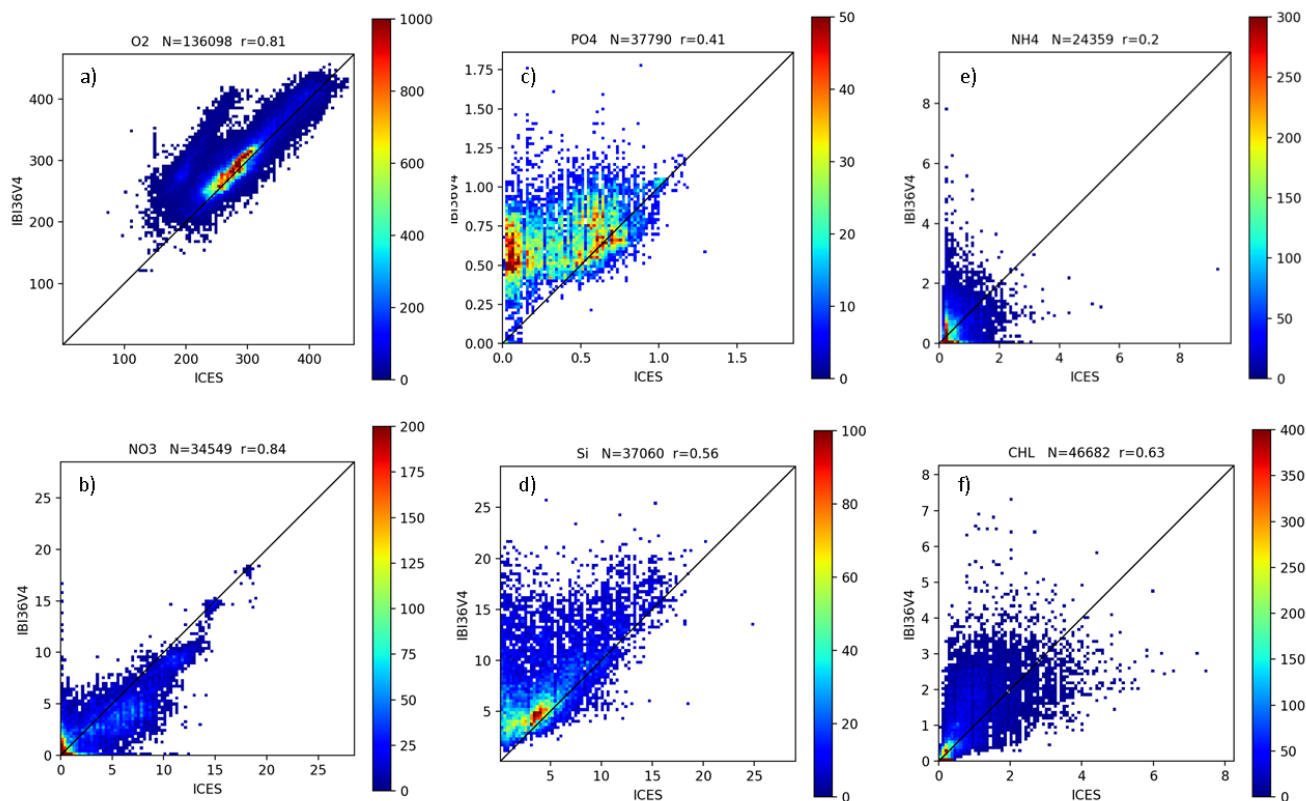
Figure 7. Density plots for oxygen (a), nitrate (b), phosphate (c), silicate (d), ammonium (e), and Chl-a (f). ICES data are on the x-axis and IBI36 on the y-axis. Oxygen and nutrients are expressed in µmol l^{-1} and Chl-a in mg Chl m^{-3}. Each axis is divided in 100 bins and colorbar represents the density of the match-ups (number of overlapping points). Note the different scales for the variables. Low density points are removed (density lower than the threshold of 5), some extrema are then not visible here. N indicates the total number of match-ups, and r the Pearson correlation coefficient. IBI36 and ICES data are collocated in space and time between 2010 and 2016. All depths are presented, keeping in mind that ICES data are mainly located in the shallow and coastal waters of the Northern seas.
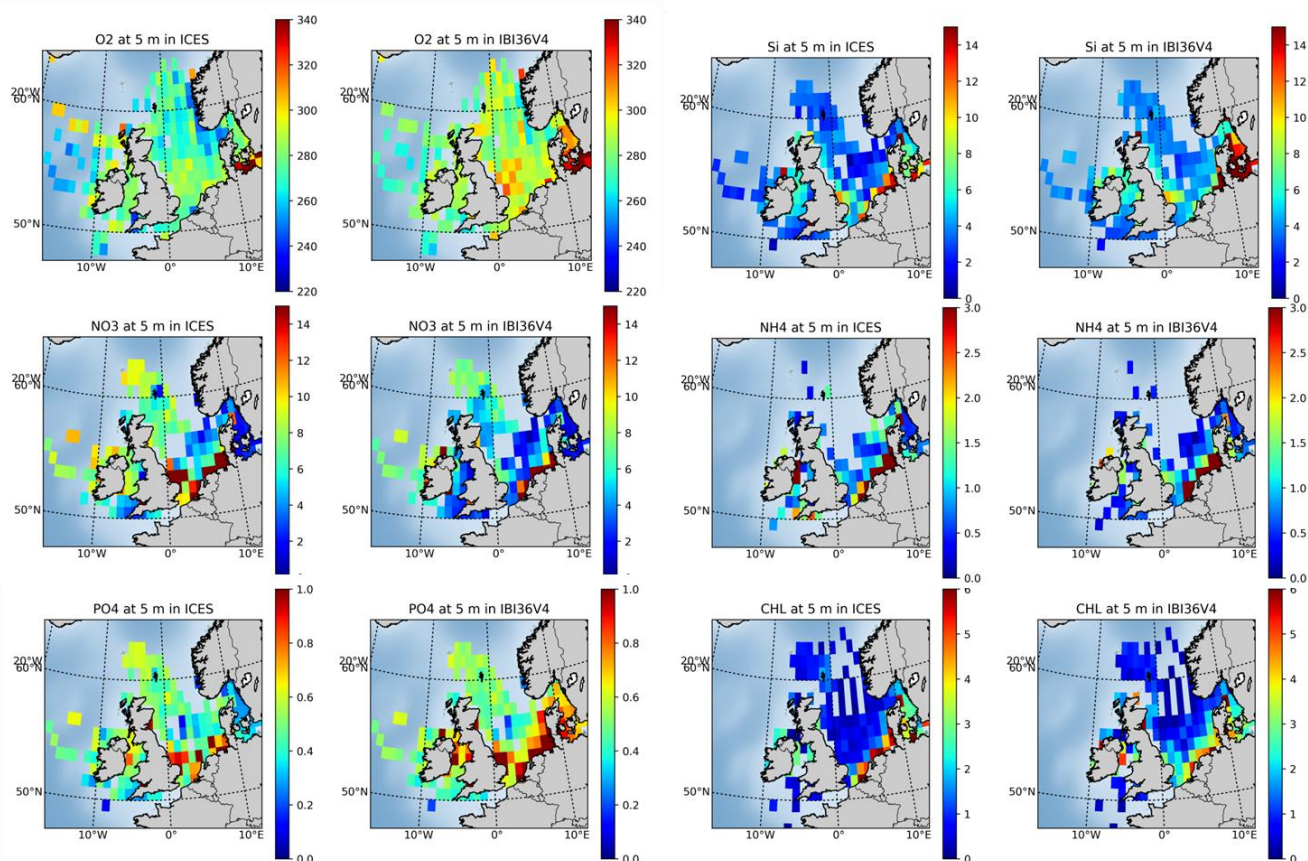
5

Figure 8. Surface concentrations of oxygen, nitrate, phosphate, silicate, ammonium and Chl-a from ICES database and IBI36. Oxygen and nutrients are expressed in µmol l^{-1} and Chl-a in mg Chl m^{-3}. IBI36 and ICES data are collocated in space and time between 2010 and 2016. Match-ups are averaged between 0 and 10 meter depth, gridded and averaged on a horizontal grid of 1°x1° resolution. Grid points containing less than 5 data are excluded.
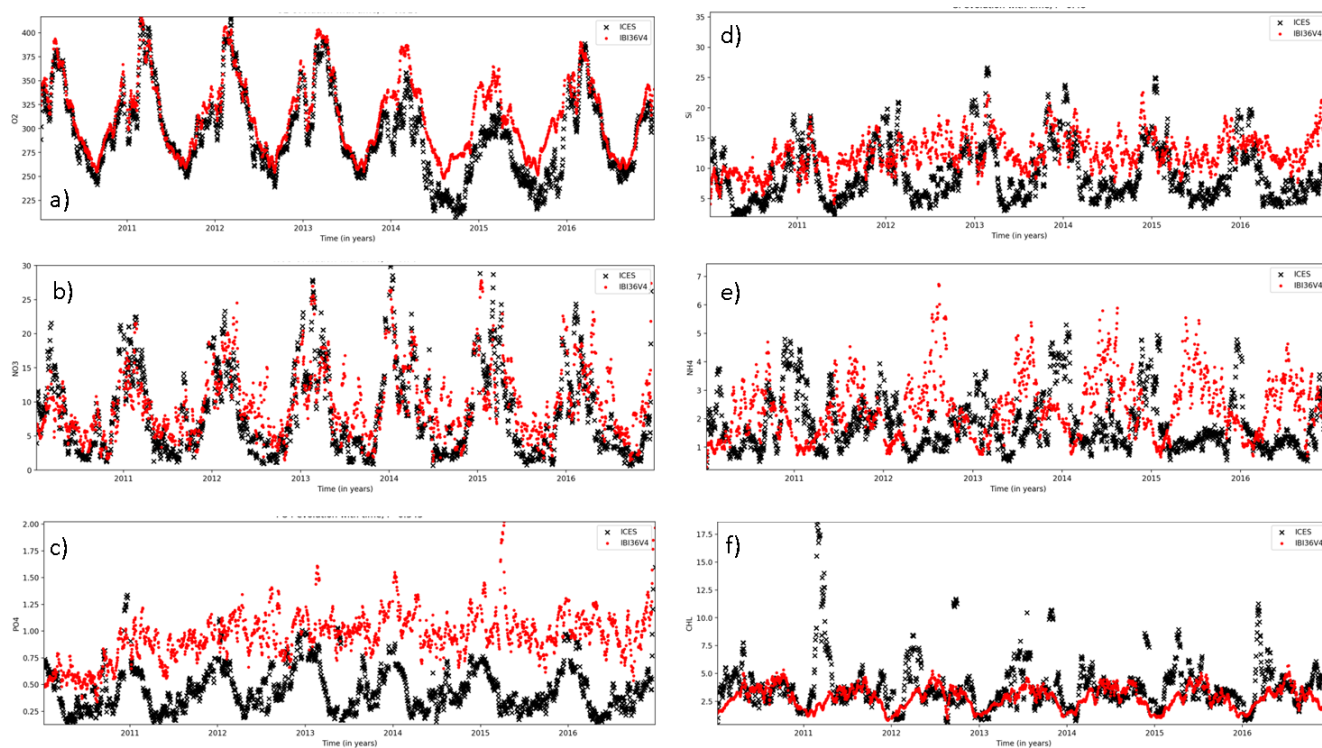
10

5

Figure 9. Time series of surface concentrations of a) oxygen, b) nitrate, c) phosphate, d) silicate, e) ammonium and f) Chl-a from ICES (black) and IBI36 (red). Oxygen and nutrients are expressed in µmol l^{-1} and Chl-a in mg Chl m^{-3}. IBI36 and ICES data are collocated in space and time between 2010 and 2016. Match-ups are averaged between 0 and 10 meter depth, and
10 daily averaged. Time series are smoothed using a 10-day window.
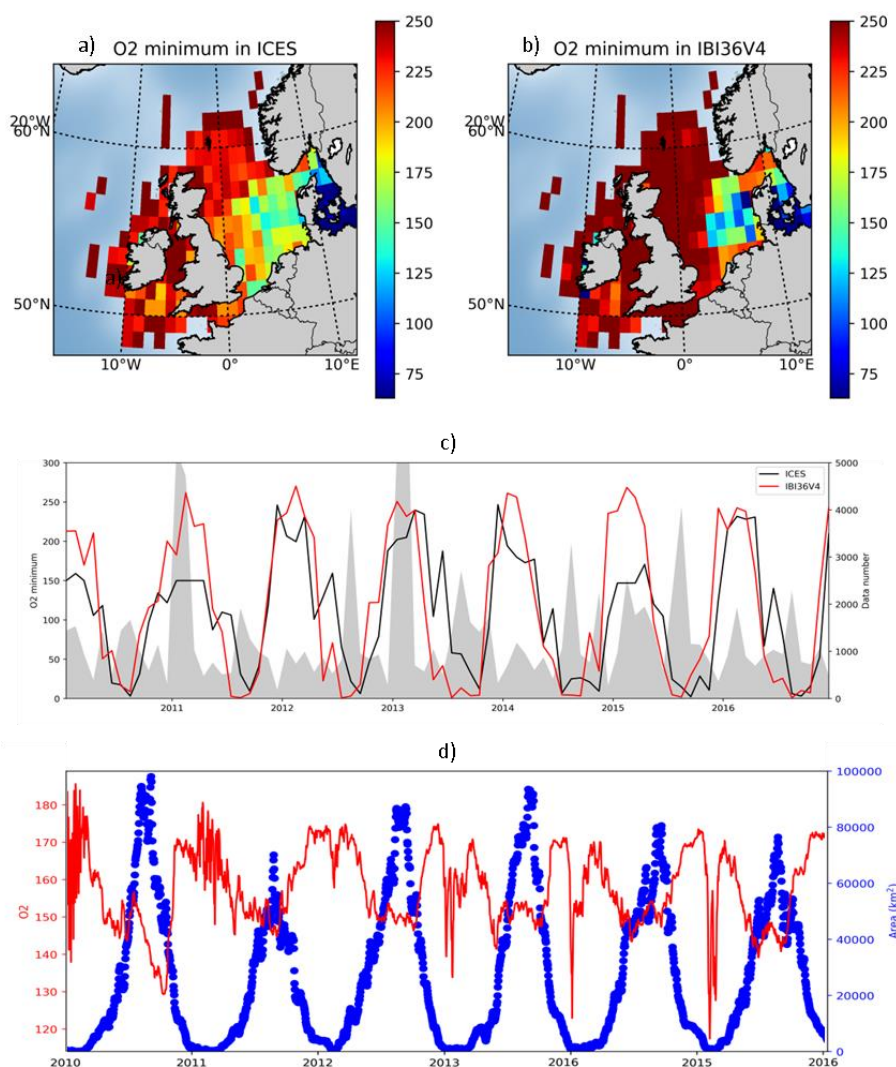
Figure 10: Areas vulnerable to oxygen deficiency over the continental shelf (bathymetry <= 200m). Minimum oxygen (μmol l^{-1}) in a) ICES data and b) IBI36. c) Time series of minimum oxygen (μmol l^{-1}) in ICES data (black) and IBI36 (red). Number of available data in ICES is added to the right axis (area plot in gray). d) Surface area (in km^2) where oxygen concentrations decrease below the threshold of 6 mg l^{-1} (or 187.5 μmol l^{-1}) over the continental shelf (blue; right axis) and associated mean oxygen concentrations (μmol l^{-1}; red; left axis) in IBI36.

10

5
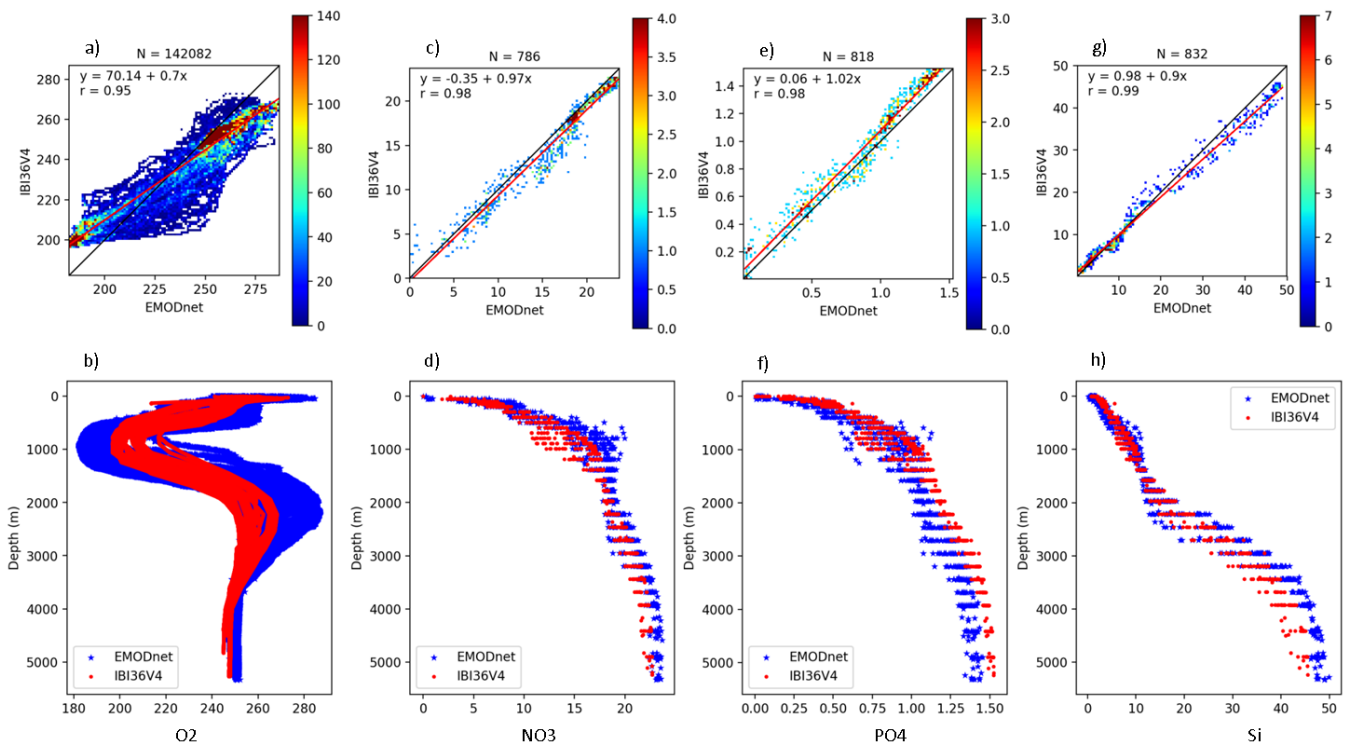
Figure 11. Density plots (top) and vertical profiles (bottom) for oxygen (a, b), nitrate (c, d), phosphate (e, f), and silicate (g, h) from OVIDE section data (EMODnet database) and IBI36. All nutrients are expressed in μmol l^{-1}. OVIDE data are on the x-axis and IBI36 on the y-axis of the density plots. Each axis is divided in 100 bins and colorbar represents the density of the match-ups (number of overlapping points). Note the different scales for the variables. N indicates the total number of match-ups, and r the Pearson correlation coefficient. IBI36 and OVIDE section data are collocated in space and time.
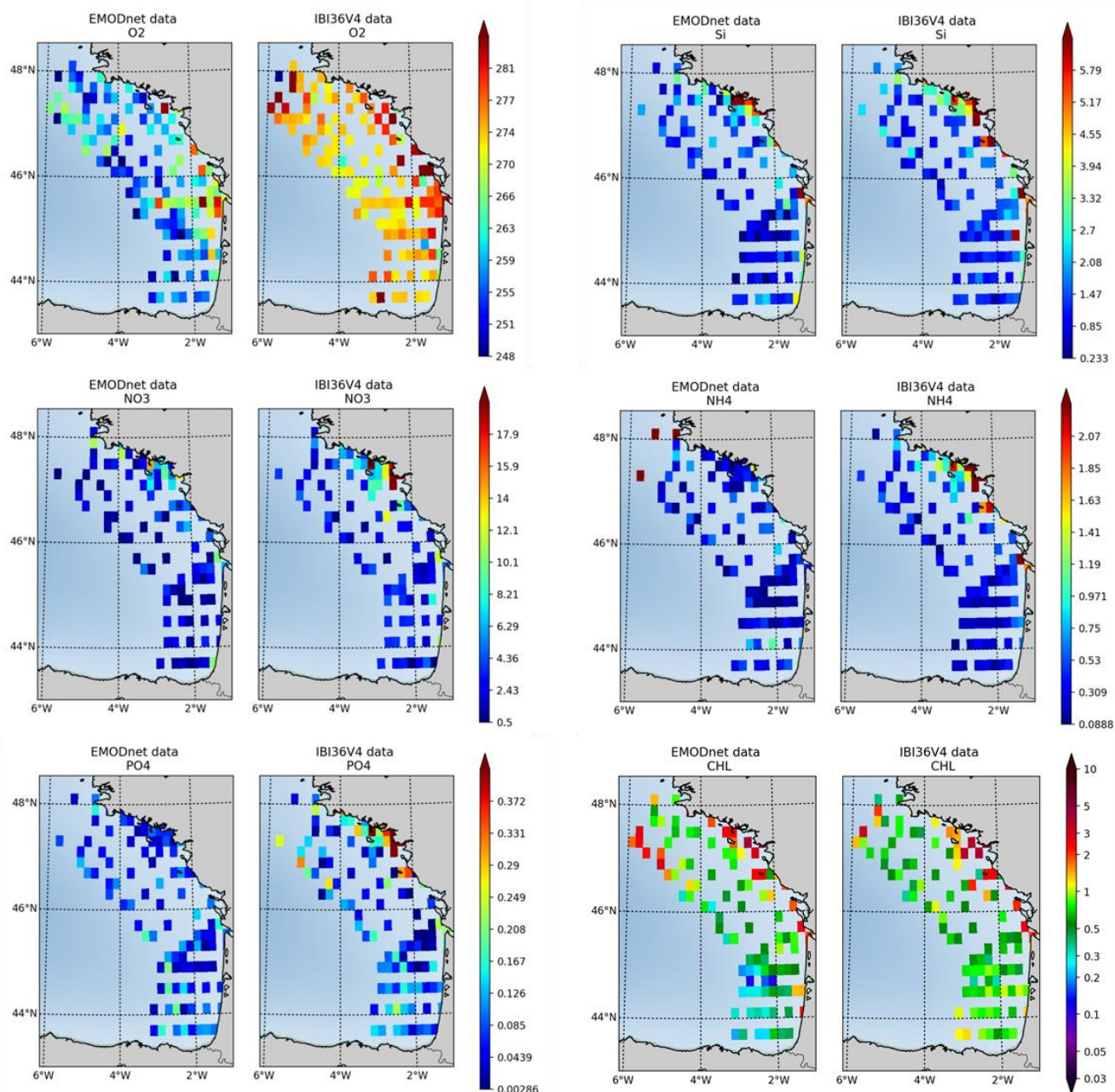
Figure 12. Surface concentrations of oxygen, nitrate, phosphate, silicate, ammonium and Chl-a from PELGAS data (EMODnet database) and IBI36. Oxygen and nutrients are expressed in µmol l^{-1} and Chl-a in mg Chl m^{-3}. IBI36 and PELGAS data are collocated in space and time between 2010 and 2016. Match-ups are averaged between 0 and 10 meter depth, gridded and averaged on a horizontal grid of 0.1°x0.1° resolution.

35

Ocean Science
Discussions

Open Access

EGU

5
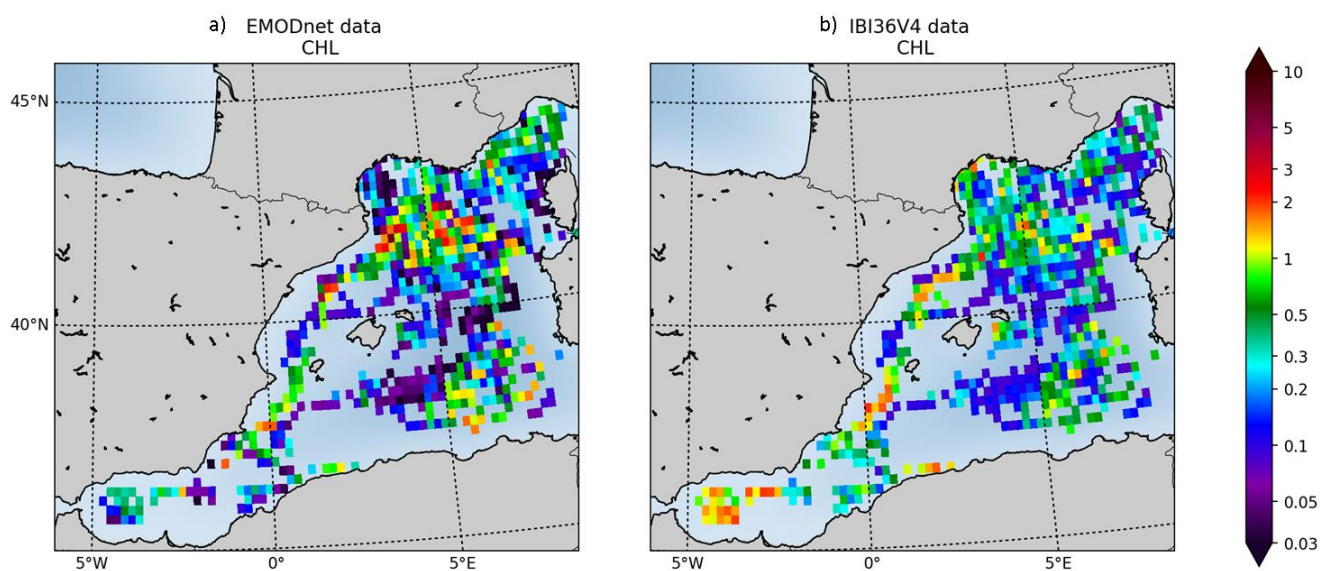
10

Figure 13. Sea surface Chl-a from EMODnet data (a) and IBI36 (b) in mg Chl m^{-3}. IBI36 and EMODnet data are collocated in space and time between 2010 and 2016. Match-ups are averaged between 0 and 10 meter depth, gridded and averaged on a horizontal grid of 0.2°x0.2° resolution.
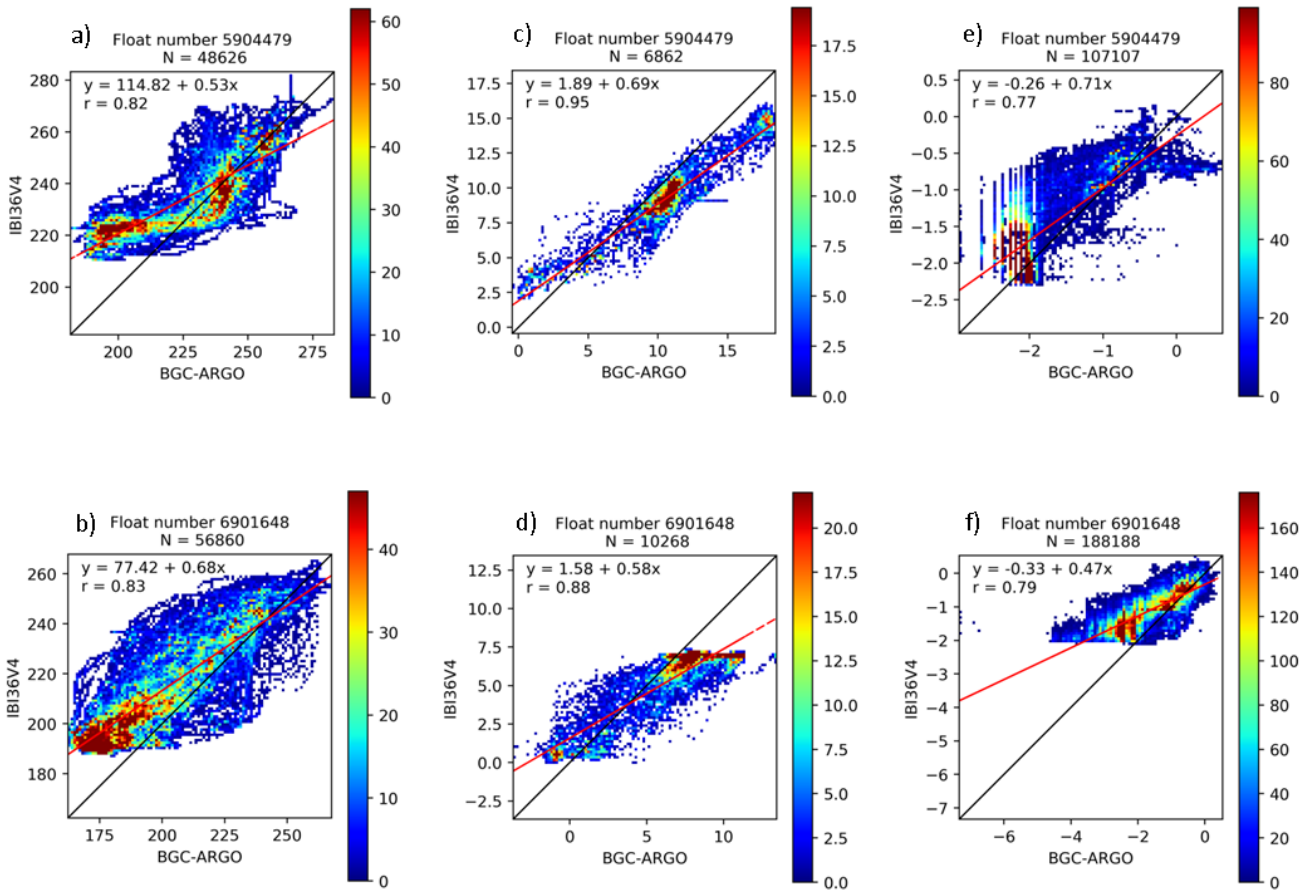
Figure 14. Density plots for oxygen (a, b), nitrate (c, d), and log(Chl-a) (e, f) from BGC-Argo data and IBI36 for the Atlantic (top) and Mediterranean (bottom). Oxygen and nitrate are expressed in µmol l^{-1}. Argo data are on the x-axis and IBI36 on the y-axis of the density plots. Each axis is divided in 100 bins and colorbar represents the density of the match-ups (number of overlapping points). Note the different scales for the variables. N indicates the total number of match-ups, and r the Pearson correlation coefficient. IBI36 and Argo data are collocated in space and time.
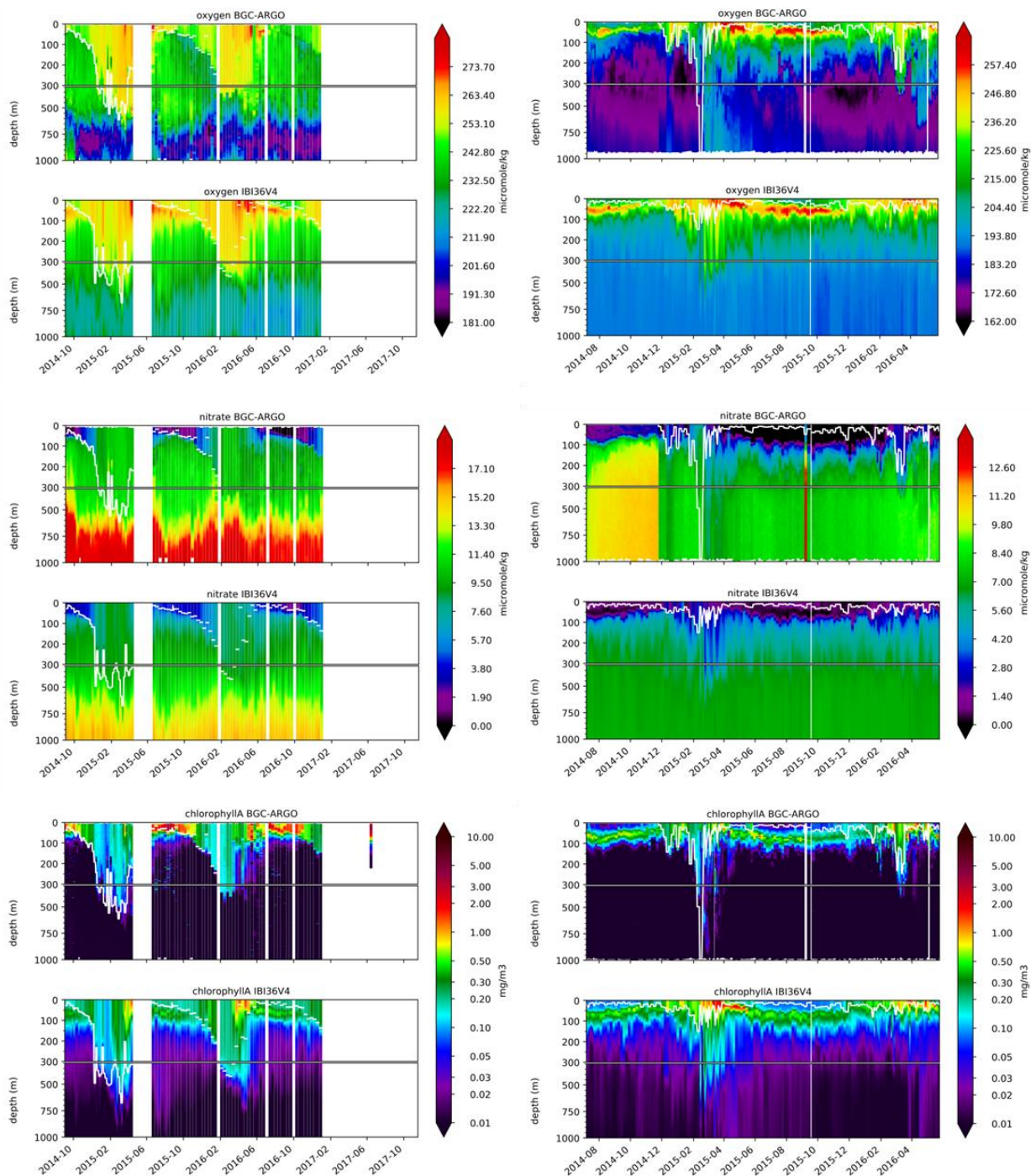
Figure 15. Time series of oxygen (top), nitrate (middle), and Chl-a (bottom) from BGC-Argo data and IBI36 for the Atlantic (left) and Mediterranean (right). Oxygen and nitrate are expressed in μmol l^{-1} and Chl-a in mg Chl m^{-3}. IBI36 and Argo data are collocated in space and time.